UNIVERSITY OF OKLAHOMA

GRADUATE COLLEGE

STRATIGRAPHIC VARIABILITY OF MINERALOGY, ROCK TYPES, AND POROSITY OF THE WOLFCAMP FORMATION USING MULTI-MINERAL PETROPHYSICAL ANALYSIS AND SEISMICALLY CONSTRAINED RESERVOIR MODELING, NORTHWEST SHELF, DELAWARE BASIN

A THESIS

SUBMITTED TO THE GRADUATE FACULTY

in partial fulfillment of the requirements for the

Degree of

MASTER OF SCIENCE

By

LINDY M.
DINGMORE
Norman, Oklahoma
2020

Downloaded from SHAREOK. Persistent Handle URL: https://hdl.handle.net/11244/325305

STRATIGRAPHIC VARIABILITY OF MINERALOGY, ROCK TYPES, AND POROSITY OF THE WOLFCAMP FORMATION USING MULTI-MINERAL PETROPHYSICAL ANALYSIS AND SEISMICALLY CONSTRAINED RESERVOIR MODELING, NORTHWEST SHELF, DELAWARE BASIN

A THESIS APPROVED FOR THE
SCHOOL OF GEOSCIENCES

BY THE COMMITTEE CONSISTING OF

Dr. Matthew Pranter, Chair

Dr. John Pigott

Dr. Zulfiquar Reza

© Copyright by LINDY M. DINGMORE 2020
All Rights Reserved.

Acknowledgements

I thank Devon Energy for providing well-log and 3D-seismic data and Schlumberger (Petrel), Emerson Paradigm (Geolog), CGG (HampsonRussell), and the OU Attribute Assisted Seismic Processing and Interpretation Consortium (AASPI) for software. I would like to thank Dr. Reza and Dr. Pigott for both their patience and guidance. I would like to especially thank Dr. Pranter for his support and faithful commitment. He has been a leading example of countless admirable qualities as a geologist, advisor, and mentor that I hope to one day be. I thank all my fellow researchers with their technical assistance and encouragement. Lastly, I would like to thank my mom and dad for always believing in me and Carson for helping me never give up on my dreams.

TABLE OF CONTENTS

ACKNOWLEDGEMENTS iv

ABSTRACT vii

INTRODUCTION 1

GEOLOGIC SETTING 5

METHODS 9

Estimating Petrophysical and Geomechanical Properties, Mineralogy, and Rock Types 9

Stratigraphic and Structural Framework 16

Post-Stack Inversion 17

3D Reservoir Modeling 21

RESULTS 24

Petrophysical and Geomechanical Properties, Mineralogies, and Rock Types 24

Stratigraphic and Structural Framework 25

P-Impedance, Rock types, and Porosity Trends 26

Spatial Distribution of Rock types, Petrophyscial and Geomechanical Properties 38

DISCUSSION 51

Rock Types and Petrophysical and Geomechanical Properties related to Reservoir Quality 51

Utilizing ρ_{maa}-u_{maa} Interpretation of Mineral Composition 52

Limitations 53

CONCLUSIONS 53

REFERENCES 56

APPENDIX A: Geologic Setting..... 61

APPENDIX B: Shale Index Baselines..... 62

APPENDIX C: Cumulative Hydrocarbon Pore Thickness Calculation..... 63

APPENDIX D: Seismic Data..... 64

APPENDIX E: P-Impedance Trend Volumes..... 67

APPENDIX F: Pay Distribution..... 68

ABSTRACT

The Wolfcamp Formation on the Northwest Shelf of the Delaware Basin formed in a low-angle (<1˚) slope-to-basin depositional environment and is primarily composed of sediment gravity flows. Multi-scale heterogeneities within the Wolfcamp are reflected in its stratigraphic architecture, rock types, petrophysical properties, and their spatial distribution. The Wolfcamp Formation is informally divided into four stratigraphic zones, from top to bottom Zones A, B, C, D, in which reservoir quality was analyzed. Seismic-constrained 3D reservoir modeling was used to map the Wolfcamp mineralogy, rock types, and petrophysical and geomechanical properties to explore their spatial distribution and relate these parameters to hydrocarbon pore volume.

The study area is west of Carlsbad, New Mexico and data include a 93 mi^2 (240 km^2) 3D seismic survey and logs from 45 wells within the survey that penetrate the entire Wolfcamp Formation. Across the study area, the Wolfcamp Formation gradually dips to the east-southeast or basinward, varies in elevation from -4764 to -5600 ft (-1454 to -1706 m), and varies in thickness from 106 to 1206 ft (32 to 367 m). Each stratigraphic zone displays proportional thickening in the depositional dip direction to the southeast.

For the Wolfcamp Formation in the study area, shale volume (V_{sh}) ranges from 0-100% with an average ~30%. Higher values of V_{sh} are common in the lower and middle Wolfcamp Formation. Total and effective porosity (ϕ_t and ϕ_e) for the Wolfcamp Formation both range from 0-16% and average ~10% and 4%, respectively. ϕ_t and ϕ_e vary stratigraphically and general are higher in dolomites and lower in limestones. Average water saturation (S_w) is 35%, ranges from 0 to 100%, and increases moving stratigraphically upward. Lower values of S_w generally correspond to dolomite and high values vary between limestones and sandstones.

Based on ρ_{maa}-U_{maa} analysis and a V_{sh} cut-off, the Wolfcamp Formation has 29% mudstone, 27% limestone, 22% sandstone, and 22% dolomite. The stratigraphic distribution of rock types reflects the variability in mineral composition for the Wolfcamp Formation. The base of the Wolfcamp is primarily mudstone and mudstone percent decreases upward through the section. Limestone and dolomite percentages are greatest in Zones B and C, respectively. Sandstone percent is low in lower and middle Wolfcamp and is dominant in the upper Wolfcamp.

Relationships between rock types and specific ranges in p-impedance values were established and used to map the distribution of rock types. 3D rock-type and petrophysical property models illustrate how reservoir quality varies by rock type and reservoir zone. Dolomites exhibit the highest effective porosity and hydrocarbon pore volume and poor reservoir quality is associated with limestones. Zone C has low S_w, relatively high brittleness index, contains a high proportion of dolomite, and would be an optimal interval to land horizontal wells for development.

INTRODUCTION

The Permian Basin located in west Texas and southeastern New Mexico covers approximately 53 million ac (214,483 km^2) and contains more than 7,000 fields producing from numerous Permian aged formations (U.S. Department of the Interior, 2018). Within the Permian Basin, the Delaware Basin has significant development from the Bone Spring and Wolfcamp formations. Previously assessed as a vertical target, advancement of unconventional drilling has been successful in the Wolfcamp. The Wolfcamp Formation in the Delaware Basin is largely an unconventional play with a median hydrocarbon mix of 60% light crude (>40.1 degrees API), 20% wet gas and 20% dry gas (University of Houston Energy, 2019). The U.S. Geologic Survey in 2018 estimated an average of 46.3 billion barrels of oil, 281 trillion cubic feet of natural gas and 20 billion barrels of natural gas liquids of potential reserves within the Bone Spring and Wolfcamp formations, Delaware Basin. By providing additional insight to the stratigraphic variability and spatial distribution of reservoir quality, this study is relevant to hydrocarbon development strategies.

The Wolfcamp Formation on the Northwest Shelf of the Delaware Basin (Figure 1) formed in a low-angle (<1˚) slope-to-basin depositional environment and is primarily composed of carbonate and clastic sediment gravity flows (Cook, 1983; Kvale et al., 2020). During the Wolfcampian a large carbonate channel-to fan complex developed in the northern Delaware Basin (Janson et al., 2019). Under normal sea-level conditions, the shelf margin formed close to sea level, providing a shallow broad backreef, restricting terrigenous sands from the distal basin (Silver and Todd, 1969). As sea level fell, clastic sands were deposited into the basin via submarine fan depositional processes (Cook, 1983). When sea level began to rise again, the carbonate shelf became active building up the barrier reef thus restricting the amount of clastic

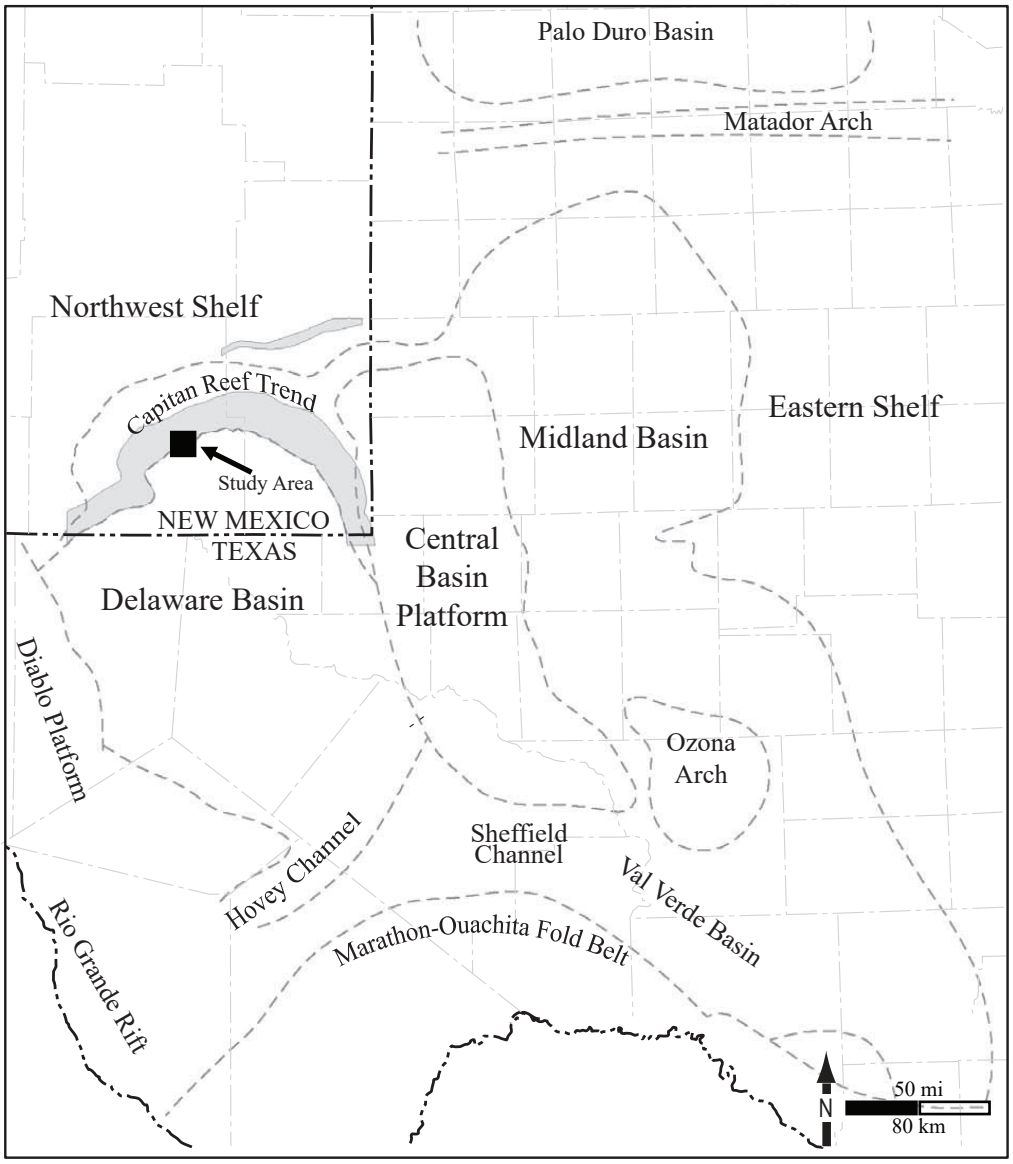


Figure 1: Geologic province of the Permian Basin in west Texas and southeastern New Mexico. The study area is marked by the black square near the Northwest Shelf, Delaware Basin (figure modified from Silver and Todd, 1969; Hills, 1984; Frenzel et al., 1988; Kosters et al., 1989; Ewing et al., 1990; Kerans and Fitchen, 1995; Moede, 2018).

sediment to the basin (Silver and Todd, 1969). The Wolfcamp Formation in Eddy County, New Mexico has been shown to consist primarily of debris flows with orthoconglomerates having a calcareous siliciclastic mudstone matrix (Loucks et al., 1985).

Kvale et al. (2020) studied the facies variability within a mixed carbonate-siliciclastic sea-floor fan of the upper Wolfcamp Formation in the Delaware Basin in southeast New Mexico (proximal to the study area). Three cores approximately 350 ft (100 m) thick, were collected that represent the frontal-to-distal fringe, off axis and lateral fringe parts of the fans. Through core description the Wolfcamp displays high stratigraphic and lateral variability in facies. The distribution of favorable reservoir facies was identified in part by measured estimates of porosity and permeability associated with the argillaceous siltstones and mudstones facies. The distribution of reservoir facies was mapped by constructing net carbonate percentages (using a gamma ray cut off) for stratigraphically defined intervals due to an inverse relationship between carbonate cement and reservoir facies. This resulted in a fan shaped lobe trending from northeast-southwest and sourced from the northeast. The net-to-gross carbonate percentage is highest in the axial part of the fan and decreases outwardly. Kvale et al. (2020) concludes the carbonate-siliciclastic deep-water fans of the Wolfcamp Formation are largely undocumented however their geometries can successfully be mapped using net-to-gross carbonate percentage to develop enhanced exploration strategies within the Delaware Basin (Kvale et al., 2020).

Cross-plots of apparent matrix grain-density versus apparent matrix volumetric cross-section (ρ_{maa}-U_{maa} cross-plots) are a type of multi-mineral, litho-density analysis and are specifically used for mineral composition identification. The method uses neutron, density, and photoelectric factor logs and is useful in formations with complex mineralogies, with variable grain densities in which porosity estimation is challenging (Theologou et al., 2015). Based on

mineral composition from ρ_{maa}-U_{maa} analysis, Wolfcamp Formation lithologies in the area primarily include mudstones, sandstones, limestones, and dolomites (Loucks et al., 1985). Dommisse et al. (2018) successfully used the method of mineral interpretation using ρ_{maa}-U_{maa} analysis on the Spraberry and Wolfcamp formations in Midland Basin. The ρ_{maa}-U_{maa} analysis for 700 wells were compared to multi-mineral facies classifications and the interpretation was consistent with the geologic framework and core data measurements. As a result, the estimated mineral compositions and proportions contributed to exploring the influence of geologic trend on productivity within the Midland Basin (Dommisse et al., 2018). In addition to mineral identification, ρ_{maa}-U_{maa} analysis provides an estimate of mineral volumetric proportion. For the San Andres Formation in Vacuum Field, New Mexico, anhydrite commonly occurs in intervals with mixed lithologies and variable porosity, making reservoir quality difficult to map (Pranter et al., 2004). ρ_{maa}-U_{maa} analysis was used to quantitatively estimate anhydrite composition and proportion to accurately map its distribution, as well as reservoir quality. This method was preferred over single density logs or density-neutron cross-plots because a combined use of photoelectric factor, density, and neutron logs help to resolve more variables (Pranter et al., 2004).

To build upon these types of studies, this study further explores the mineralogy, rock types, and petrophysical and geomechanical properties associated with sediment gravity flows of the Wolfcamp Formation for an area of the Northwest Shelf. The spatial distribution of rock types, porosity, water saturation, and brittleness index are determined by integrating well-log and 3D seismic data. For the Wolfcamp Formation for this area of the Northwest Shelf, Delaware Basin, this study addresses the following questions:

1. What are the dominant mineralogies and rock types?
2. What is the stratigraphic architecture (reservoir zones)?
3. How do seismic amplitudes and acoustic impedance relate to rock types and porosity?
4. What is the stratigraphic variability of rock types, porosity, water saturation, and brittleness index associated with the reservoir zones?

The study area covers a 93 mi^2 (240 km^2) area of Eddy County, New Mexico. Data include 45 wells that penetrate the entire Wolfcamp Formation, 20 wells with quad-combo log suite (gamma-ray, neutron and density porosity, bulk density, and resistivity), 10 wells with photoelectric factor and computed p-impedance logs, and the remaining wells contain various LAS files. In addition to well-log data, the study area is covered by a 93 mi^2 (240 km^2) 3D seismic survey that contains bin size of 82.5 ft (25 m) (Figure 2). This study includes petrophysical analysis using multi-mineral ρ_{maa}-U_{maa} cross-plots to determine log-defined rock types. Brittleness index is calculated using the mineral volumetric proportions from the multi-mineral analysis. The stratigraphic framework was defined using well-log and seismic data. Well data were used to illustrate relationships between rock types, p-impedance, and porosity. A 3D post-stack seismic inversion was conducted to derive a p-impedance volume to guide the spatial distribution of rock types. Significant petrophysical and geomechanical properties of the Wolfcamp debris flows was explored using seismic-constrained 3D reservoir models.

GEOLOGIC SETTING

The Northwest Shelf and basin margins of the Permian Basin were well defined before Permian time (Oriel et al., 1967). The Permian Basin located in west Texas and southeast New Mexico formed from advanced basin development of the ancestral Tobosa Basin (Galley, 1958).

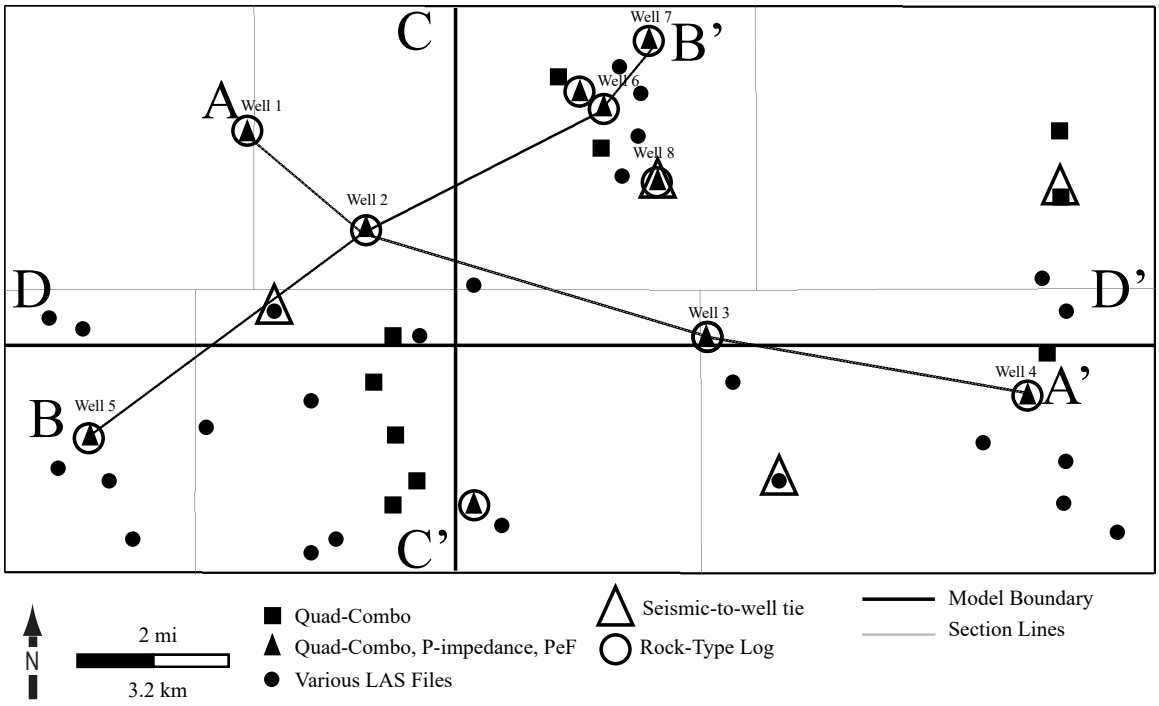


Figure 2: Detailed basemap showing 45 vertical well locations model profiles and well-log cross sections of interest. Data for the study area include a 3D seismic survey that corresponds to the model boundary. Well-log data for 45 wells that penetrate the entire Wolfcamp Formation consist of 20 wells with quad-combo log suite (gamma-ray, neutron and density porosity, sonic, bulk density, and resistivity), 10 wells with photoelectric factor and p-impedance logs, and the remaining wells contain various LAS files. Well 3 indicates the location of the type well for this study. Well-log cross sections A-A' and B-B' are shown in Figure 8. Section C-C' is shown as Figure 5. Modeled sections D-D' are shown as Figures 18 and 19. Study area location is shown in Figure 1.

The ancestral basin formed on a flat cratonic platform (present day North America) made up of broad open structures (Galley, 1958). Uplift of the Marathon-Ouachita Mountains during the Pennsylvanian through the early Permian defined the eastern and southern border of the Permian basin. Regional uplift shed large amounts of siliciclastic material into the Permian basin (U.S. Department of Energy, 2018). During the late Pennsylvanian, uplift of the Central Basin Platform and the Diablo Platform emphasized the sub-basin components of the Permian Basin; i.e., Delaware Basin, Midland Basin, Central Basin Platform, Northwest Shelf and Eastern Shelf (Figure 1, Galley, 1958).

During the early Permian, the Delaware Basin was structural bounded by the uplifting Diablo Platform to the west, the uplifting Central Basin Platform to the east, the Northwest Shelf to the north-northwest, and the Marathon Ouachita Mountains to the south (Yang and Dorobek, 1995). As the bounding uplifts continued rising, increased rate of subsidence provided accommodation for sediments that were being shed into the basin by submarine fan depositional processes forming debris flows and turbidite deposits (Cook, 1983; U.S. Department of Energy, 2018). Allochthonous carbonates comprise the deposits that form wackestone to packstone calcarenite turbidities with biotic grains (Cook, 1983). Wolfcamp outcrops studied by Playton and Kerans (2002) estimate the localized paleo-water depth in the Delaware Basin was greater than 1000 ft (300 m) (Appendix A).

The depositional interpretation during the lower Permian follows a reciprocal model of sedimentation. The reciprocal model refers to siliciclastics deposition during lowstands and carbonate deposition during highstands (Handford, 1981). This provided the presence of siliciclastic sediment in basin-floor fans during times when sea level fell below the shelf and the presences of carbonate sediments near the basin margin (transported by carbonate debris flows

from the shelf platform) during times when sea level was above the shelf (Handford and Loucks, 1993; Kvale et al., 2020).

The Early Permian Wolfcamp Formation overlies the Pennsylvanian Cisco Formation. The Cisco Formation represents early development of a carbonate shelf in the northern portion of the Delaware Basin (Adams, 1965). The contact between the two formations is the Pennsylvanian-Permian unconformity. As tectonic motion and the rate of subsidence began to decrease throughout the late Wolfcampian, the carbonate shelf and rimmed edges began to develop in shallow warm waters in the northern Delaware Basin (Adams, 1965). The Wolfcamp Formation was deposited across the Delaware Basin, Central Basin Platform, and the Midland Basin with the thickest accumulation in the Delaware Basin (Vertrees et al., 1953; Gaswirth, 2017; U.S. Department of Energy, 2018).

The Delaware Basin was filled with deposits that are Wolfcampian, Leonardian, Guadalupian, and Ochoan in age. Directly overlying the Wolfcamp Formation is the Leonardian Bone Spring Formation which is characterized by reciprocal sedimentation with alternating carbonate deposition during highstand periods and clastic deposition during lowstand periods (Bickley, 2019). During the Guadalupian, the shelf became more defined thus increasing the carbonate development on the shelf margin. Over time, the reef development resulted in restricting the Delaware Basins environment (Adams, 1965). By the end of the Permian during the Ochoa, the Delaware Basin was a completely restricted environment comprised of evaporitic lagoons and was capped by a thick layer of evaporite known as the Castile Formation (Adams, 1965).

METHODS

Estimating Petrophysical and Geomechanical Properties, Mineralogy, and Rock Types

Mineralogy, rock types, and petrophysical and geomechanical properties were calculated to assess their variability and spatial distribution in the Wolfcamp Formation. All gamma-ray and neutron porosity logs were normalized to Well 3 (Figure 3) in the study area before petrophysical properties were calculated. The caliper log was used to quality check erroneous data indicated by log spikes (>12 in; 30 cm). Spikes in the caliper log suggest borehole rugosity and zones of wash-out resulting in invalid tool measurements for pad or skid-type devices (e.g., Formation-Density Compensated: FDC^{sm}) (Market and Parker, 2011). Shale volume, total porosity, and water saturation logs were calculated using the well-log data.

Shale volume (V_{sh}; Equation 1) is calculated using the Stieber method, a two-part equation that incorporates the gamma-ray shale index (I_{sh}; Equation 2) as an input parameter (Thomas and Stieber, 1975). The baseline values (γ_{min}, γ_{max}) were identified by plotting the frequency histogram of gamma-ray logs for all 45 wells. The 10th percentile (38 API) and the 90th percentile (118 API) were defined as the sandstone and mudstone baseline values, respectively (Appendix B).

Total porosity (ϕ_t; Equation 3) is calculated as the root-mean-square of neutron and density porosity (Asquith and Gibson, 1982). Effective porosity (ϕ_e; Equation 4) is calculated using the average density porosity in a mudstone interval (identified by V_{sh} log) as opposed to the neutron porosity to minimize the potential impact of shale effect observed in the neutron porosity log. Additionally, density porosity is preferred over neutron porosity in the ϕ_e calculation because it is less sensitive to potential error in V_{sh} calculation (Bassiouni, 1994).

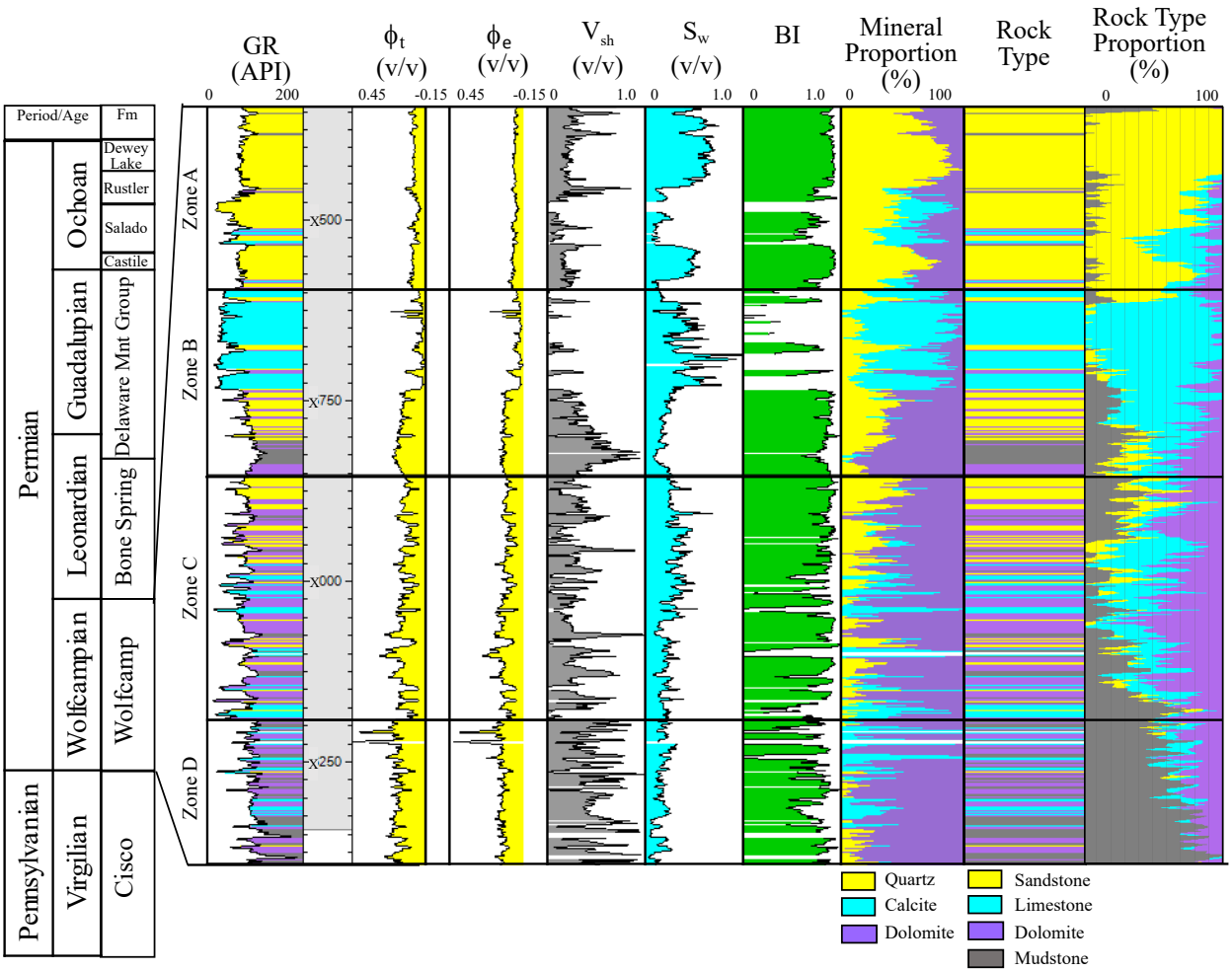


Figure 3: Generalized Permian stratigraphic column of the Northwest Shelf, Delaware Basin (Hayes, 1964) to the left corresponding to the type log with interpreted internal zones for the Wolfcamp Formation. The type well-log is tied to petrophysical and geomechanical properties, rock-type log and rock-type vertical proportion curves to the right. The rock-type vertical proportion curve illustrates the stratigraphic variability of rock types within the Wolfcamp Formation in the study area and is based on all 10 wells with rock-type logs.

Water saturation (S_w; Equation 5) is calculated using the Archie equation (Archie, 1947). Due to limited data, formation water resistivity (R_w) data was estimated based on a previous case study by Asquith (2016) that used of 0.05 Ω.m as the formation water resistivity in Archie's (1947) S_w equation for the Permian Wolfcamp. The a (1), m (2), and, n (2) parameters used were those calibrated to carbonate rocks and the porosity used was ϕ_t (Doveton, 1999).

$$V_{sh} = \frac{I_{sh}}{3-2*I_{sh}} \quad (1)$$

where,

V_{sh}, volume of shale (v/v)
I_{sh}, Shale Index (v/v)

$$I_{sh} = \frac{\Upsilon_{log}-\Upsilon_{min}}{\Upsilon_{max}-\Upsilon_{min}} \quad (2)$$

where,

I_{sh}, shale index (v/v)
Υ_{log}, gamma-ray log (API)
Υ_{min}, sandstone baseline (API)
Υ_{max}, mudstone baseline (API)

$$\phi_t = \sqrt{\frac{{\phi_D}^2+{\phi_N}^2}{2}} \quad (3)$$

where,

ϕ_t, total porosity (v/v)
ϕ_D, density porosity (v/v)
ϕ_N, neutron porosity (v/v)

$$\phi_e = \phi_t - (V_{sh} * \phi_{sh}) \quad (4)$$

where,

ϕ_e, effective porosity (v/v)
ϕ_t, total porosity (v/v)
V_{sh}, volume of shale (v/v)
ϕ_{sh}, density porosity of shale (v/v)

$$S_w = \left(\frac{a*R_w}{{\phi_t}^m*R_t}\right)^{\frac{1}{n}} \quad (5)$$

where,

S_w, water saturation (v/v)

a (1), m (1), and n (2) parameters calibrated to carbonate rocks
R_w, formation water resistivity (Ωm)
ϕ_t, total porosity (v/v)
Rt, rock resistivity (Ωm)

Well-log based, multi-mineral, litho-density ρ_{maa}-U_{maa} cross-plots were computed to estimate the types and amount of minerals that commonly comprise the Wolfcamp Formation. The relationship between ρ_{maa} and U_{maa} is derived from the bulk density (RHOB) and photoelectric factor (PeF) logs. The ρ_{maa} parameter is the apparent matrix grain density, calculated from the RHOB log (Equation 6), and U_{maa} is the apparent matrix volumetric cross-section, computed from the PeF log and calculated photo-electron density constant (Equations 7 and 8). The ρ_{maa}-U_{maa} cross-plot has an imposed ternary diagram with trend lines for quartz, calcite, dolomite (QCD) and regions for clays and anhydrites. The ρ_{maa}-U_{maa} cross-plot provides the abundance of quartz, calcite, and dolomite from the ternary diagram in volumetric proportion (%). Out of the 45 wells, 10 wells have the PeF log and were used in the multi-mineral analysis (Figure 2).

$$\rho_{maa} = \frac{\rho_b - \phi_{ta} * \rho_f}{1 - \phi_{ta}} \quad (6)$$

where,

ρ_{maa}, apparent matrix grain density (g/cm^3)
ρ_b, bulk density (g/cm^3)
ϕ_{ta}, apparent porosity (v/v)
ρ_f, flush zone pore fluid density (~1.0 g/cm^3 for fresh-water mud filtrate)

$$\rho_e = \frac{\rho_b + 0.1883}{1.0704} \quad (7)$$

where,

ρ_e, electron density (g/cm^3)
ρ_b, bulk density (g/cm^3)

$$U_{maa} = \frac{P_e \rho_e - \phi_{ta} * U_f}{1 - \phi_{ta}} \quad (8)$$

where,

U_{maa}, apparent matrix volumetric cross-section (barns/cm^3)
P_e, photoelectron index (barns/electron)
ρ_e, electron density (g/cm^3)
ϕ_{ta}, apparent total porosity (v/v)
U_f, Volumetric photoelectric absorption of the flushed zone pore fluid (~0.398 barns/cm^3)

The results of the multi-mineral analysis were used to compute well-log derived rock type logs. The ρ_{maa}-U_{maa} cross-plot determines the quartz, calcite, and dolomite abundance in volume percent. Thus, the rock type was interpreted based on the mineral with >33% of the total rock composition. The rock types derived from the ρ_{maa}-U_{maa} cross-plot consist of sandstone indicated by the quartz proportion, limestone indicated by the calcite proportion, and dolomite indicated by the dolomite proportion.

Mudstone was classified for intervals with V_{sh}>=50%. The amount of mudstone was determined separately and graphically by plotting the cumulative hydrocarbon pore thickness versus V_{sh}. The cumulative hydrocarbon pore thickness was calculated for the entire interval by multiplying different proportions of net-reservoir rock thickness, ϕ_e, and hydrocarbon saturation ($1-S_w$) by the gross thickness of the Wolfcamp interval. The net-reservoir rock thickness is the amount of reservoir rock within the total thickness of the Wolfcamp and was determined by applying different V_{sh} cut off values beginning with 0% increasing by 5% each time to 100%. For example, a 40% V_{sh} cut off would indicate any rock containing 40% or greater V_{sh} is non-reservoir rock while values below 40% V_{sh} is reservoir rock. Then the results were normalized out of 100%. The cumulative hydrocarbon pore thickness suggests the amount of reserves within the reservoir. As the amount of reserves increases, the amount of reservoir rock decreases.

Ideally, the cut off is determined by maximizing reserves while minimizing non-reservoir (in this case, mudstone) rock (Appendix C). The cross-plot of cumulative hydrocarbon pore thickness and V_{sh} show 3 different slopes whose inflection points occur at 50% and 70% V_{sh}. This is interpreted to represent 3 classes of reservoir quality associated with a decrease in reservoir quality with increasing shale (mudstone) volume. Relatively higher reservoir quality is associated with Wolfcamp intervals with <50% shale volume (mudstone). Approximately 75% of the Wolfcamp hydrocarbon pore thickness exhibits relatively higher reservoir quality. Moderate reservoir quality contains between 50-70% V_{sh}, while lower reservoir quality corresponds to intervals with V_{sh}>70%. The V_{sh} cut off used to classify mudstone rock type of the Wolfcamp is based on the inflection point from good to moderate reservoir quality; a value of 50% (Figure 4).

Brittleness index (BI; Equation 9) was calculated using a modified version of the Wang and Gale (2009) equation for BI that does not include total organic carbon (TOC) due to limited data. Mineral logs for quartz, calcite, and dolomite were derived from the ρ_{maa}-U_{maa} cross-plots (similarly to XRD data) and clay content was represented by the V_{sh} log. The 4 logs were normalized to 100%, converted from volume percent to weight percent (Equation 10), and used to calculate BI.

$$BI = \frac{Qtz+Dol}{Qtz+Dol+Cal+Clay} \quad (9)$$

where,

BI, Brittleness Index
Qtz, quartz content (W_t%)
Dol, dolomite content (W_t%)
Cal, calcite content (W_t%)
Clay, clay content (W_t%)

$$W_t\% = \frac{\rho_g * Vol\,\%}{\rho_b} \quad (10)$$

where,

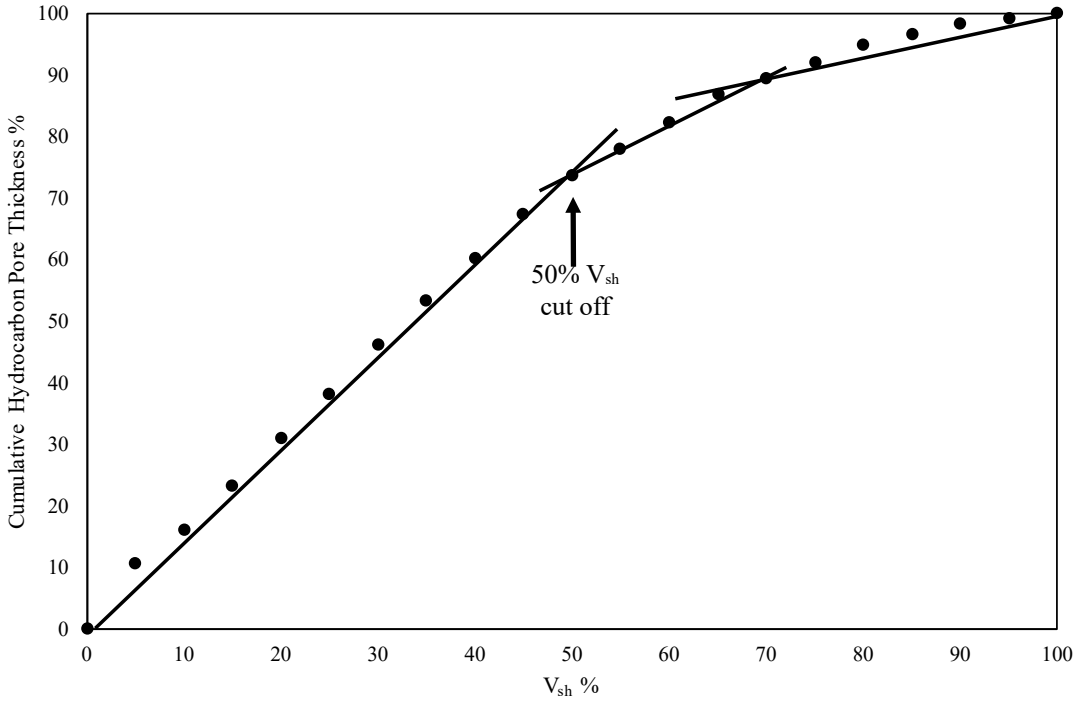


Figure 4: The cumulative hydrocarbon pore thickness versus V_{sh} cross-plot was used to determine the mudstone rock type cut off. The cross-plot illustrates 3 classes of reservoir quality associated with a decrease in reservoir quality with increasing shale (mudstone) volume. Ideally, the cut off is determined by maximizing reserves while minimizing non-reservoir. The V_{sh} cut off used to classify mudstone rock type of the Wolfcamp is based on the inflection point from good to moderate reservoir quality; a value of 50%.

W_t%, mineral weight percent (%)
ρ_g, grain density component (g/cm^3)
Vol %, mineral volume percent (%)
ρ_b, bulk density (g/cm^3)

Stratigraphic and Structural Framework

The Wolfcamp Formation stratigraphic framework and key stratigraphic surfaces were interpreted based on a 93 mi^2 (240 km^2) 3D seismic survey and log data for 45 wells that penetrate the entire Wolfcamp Formation within the seismic survey. Informally, the Wolfcamp Formation is divided into four operational zones, A-D, as described by the U.S. Department of Energy (2018); this study follows the EIA zonation for the Wolfcamp Formation. For reference, the structural elevations interpreted on well logs for the top and base of the Wolfcamp Formation were also compared to formation tops from the New Mexico Oil Conservation Division. Internal Zone tops were interpreted on well logs using trends in the rock-type log and distinct characteristics of the gamma-ray log as observed on cross-sections.

Four seismic-to-well ties (Figure 2; Appendix D) were done to relate the zone tops (in depth; SSTVD) to seismic amplitude reflectors (in time; ms) using synthetic traces. The top of the Wolfcamp and Cisco (base Wolfcamp) formations were identified in the 3D seismic survey as distinct continuous low amplitude reflectors and their horizons were mapped across the study area. A cosine of phase seismic attribute was applied to the entire volume to enhance the reflection continuity and interpretation (Barnes, 2007). The internal surfaces that define Zones B, C, and D are below seismic resolution, and those horizons were interpreted on well logs but not interpreted on seismic data (Appendix D).

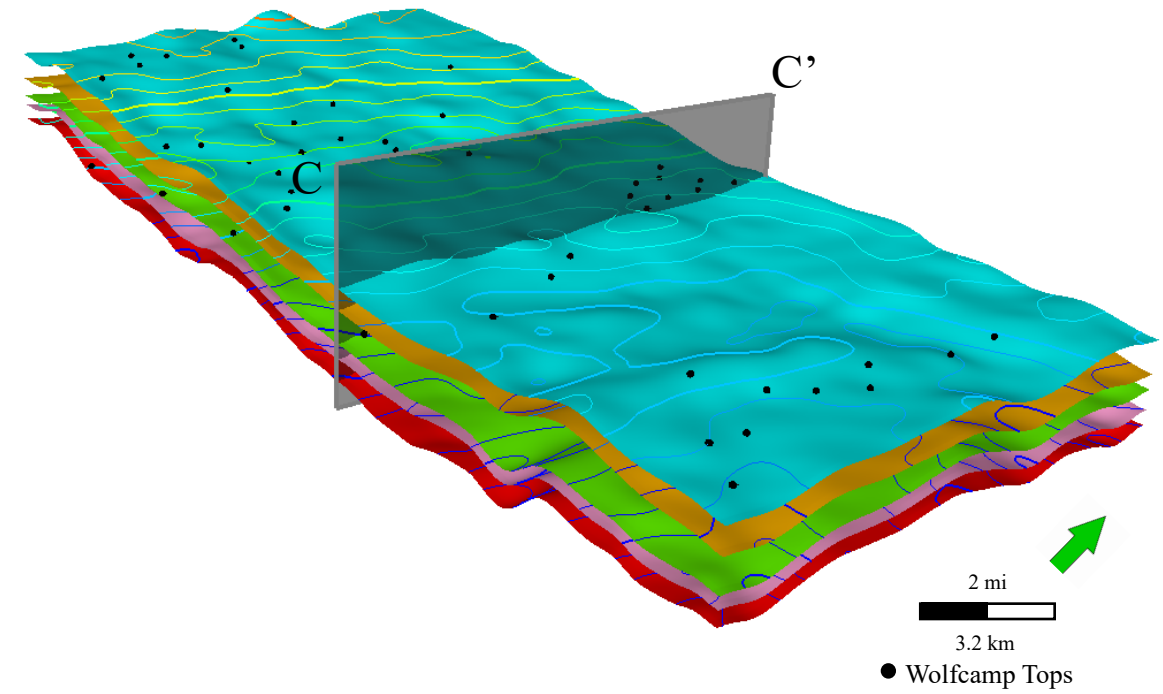
A velocity model was used to depth convert the seismic horizons in two-way-time (TWT) to depth (Z) using time-depth relationships (TDR) established from the seismic-to-well ties. The

depth converted seismic and well-top data were integrated to construct structure-contour maps for the top Wolfcamp and top Cisco (base Wolfcamp) formations. The internal structure-contour maps for Zones B, C, and D were constructed using conformal gridding. This method utilizes the top Wolfcamp and Cisco structure-contour maps as seismically constrained reference surfaces and generates structure-contour maps for the internal zones by using their well-top data while following the trends of overlying and underlying surfaces. The structure-contour map for Zone D is conformably gridded using the top Wolfcamp and Cisco as reference surfaces. The structure-contour map for Zone C is mapped using the top Wolfcamp and Zone D structure-contour maps as reference surfaces. Constructing the internal zones maps in their upward stratigraphic order provides mapping control that decreases error associated with data extrapolation, such as internal surfaces intersecting one another. This method also honors the seismically constrained surfaces (Figure 5).

Isopach maps were constructed for each zone using an isochore interpolation method. Well tops were converted into isochore points (the thickness between well tops for each zone). The minimum and maximum thickness from the well-top points of each zone were used to limit data extrapolation in areas with sparse well control.

Post-Stack Inversion

A general relationship was observed between various ranges of well-log-based p-impedance values and rock types. Therefore, a post-stack inversion was done to derive a 3D p-impedance volume that could be used to constrain the spatial distribution of rock types in the Wolfcamp Formation. P-impedance (Z_p) is a product of wave velocity (V_p) and rock density (ρ). The seismic trace (S_t) is a convolution of the wavelet and reflection coefficient (Equation 10). Assuming the seismic ray of incident is at a normal angle to the rock interface, the reflection


C
C’
2 mi
3.2 km
Wolfcamp Tops

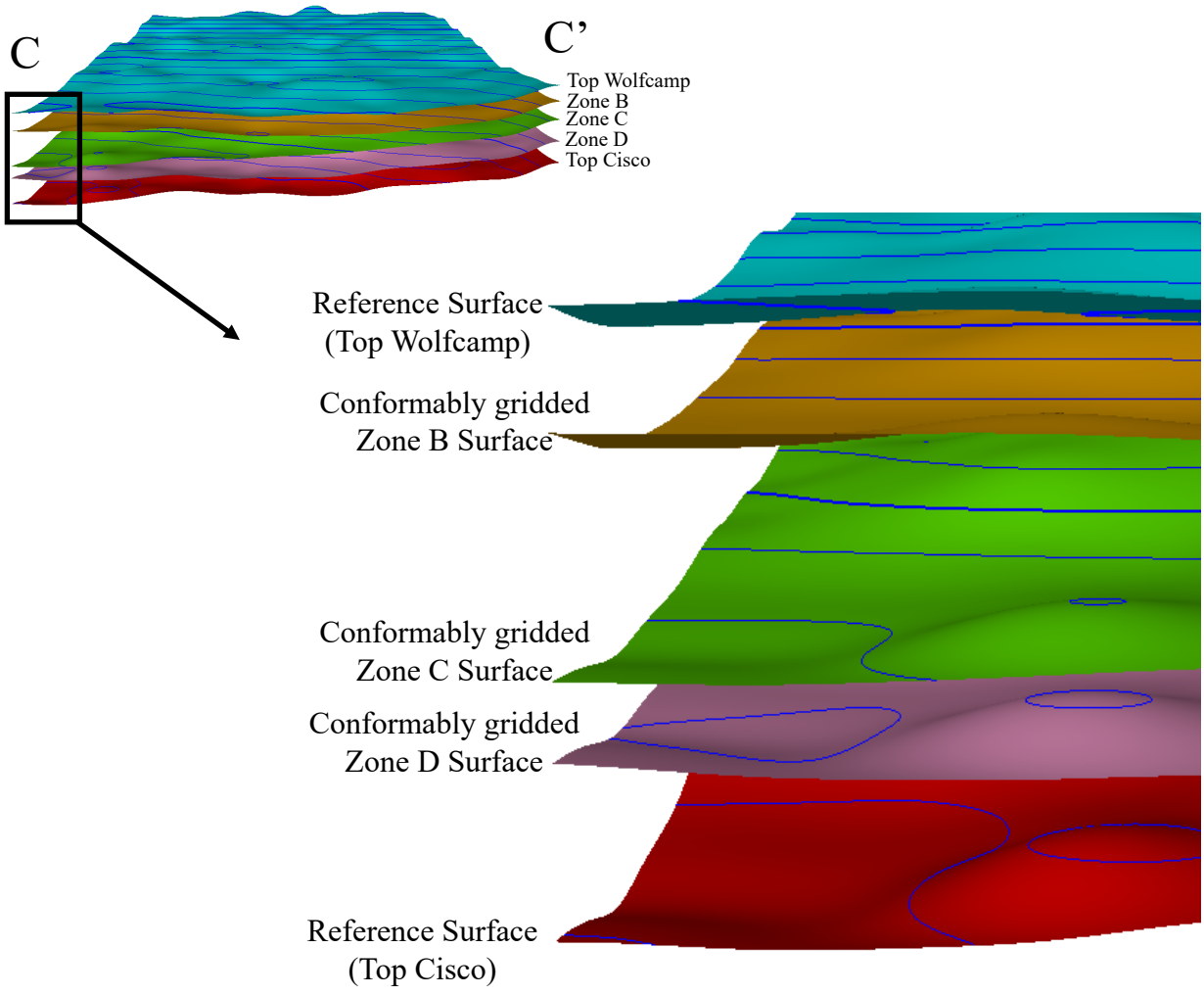

C
C’
Top Wolfcamp
Zone B
Zone C
Zone D
Top Cisco
Reference Surface
(Top Wolfcamp)
Conformably gridded
Zone B Surface
Conformably gridded
Zone C Surface
Conformably gridded
Zone D Surface
Reference Surface
(Top Cisco)

Figure 5: The structure-contour maps display depositional dip to east-southeast of the study area. The top Wolfcamp and Cisco Formation structure-contour maps were made by integrating well tops and depth-time converted seismic horizons. The internal structure-contour maps for Zones B, C, and D were constructed using conformal gridding. This method utilizes the top Wolfcamp and Cisco structure-contour maps as seismically-constrained reference surfaces, and generates structure-contour maps for the internal Zones by using their well-top data while following the trends of overlying and underlying surfaces. C-C' is a north-south cross-section through each the structure-contour maps illustrating their 3D spatial geometry.

coefficient (R_i) is equal to the p-impedance (Equation 11). The post-stack inversion reverses the forward modeling procedure by deriving an impedance volume from the reflectivity (Jafari et al., 2017). The inversion process obtains the reflection coefficient by convolving the seismic trace and inverse wavelet (Equation 12). The reconstructed p-impedance (Z_p) is then obtained by using the inverted seismic signal (Equation 13, Lindseth, 1979).

$$S_t = W_t * R_t + N_t \tag{11}$$

where,

S_t, seismic trace
W_t, seismic wavelet
R_t, reflection coefficient
N_t, noise series

$$R_i = \frac{\rho_i v_i - \rho_{i-1} v_{i-1}}{\rho_i v_i + \rho_{i-1} v_{i-1}} = \frac{Z_i - Z_{i-1}}{Z_i + Z_{i-1}} \tag{12}$$

where,

R_i, reflection coefficient of the ith layer
ρ_i, density of the ith layer (g/cc)
v_i, velocity of the ith layer (µs/ft)
Z_i, p-impedance of the ith layer (ft*s)(g/cc)

$$R_t = s_t * a_t \tag{13}$$

where,

R_t, reflection coefficient
s_t, seismic trace
a_t, inverse wavelet

$$Z_{i+1} = \rho_{i+1} v_{i+1} = \rho_i v_i \frac{1+R_i}{1-R_i} = Z_i \frac{1+R_i}{1-R_i} \tag{14}$$

where,

Z_{i+1}, p-impedance of the i+1 layer (ft*s)(g/cc)
ρ_i, density of the ith layer (g/cc)
v_i, velocity of the ith layer (µs/ft)
Z_i, p-impedance of the ith layer (ft*s)(g/cc)
R_i, reflection coefficient of the ith layer

A model-based inversion was done which uses an initial p-impedance volume that is convolved with the wavelet to obtain a synthetic response which is compared to the actual seismic signal (Figure 6). An initial background p-impedance volume was created for the Wolfcamp interval using the 4 wells. The quality of the initial volume was reviewed at each well location by analyzing the difference between the synthetic trace (computed by the inversion) to the composite seismic trace. Seismic well ties were used to extract a statistical wavelet from the Wolfcamp interval that assumed a zero phase. The wavelet was manually adjusted in 4 wells included in the volume by comparing the synthetic trace to the actual composite seismic trace. Accuracy was reviewed by checking the cross-correlation and a refined wavelet phase was extracted for each well. Once the error was appropriately reduced the final p-impedance volume was established.

A depth-converted p-impedance volume and average p-impedance map for the Wolfcamp interval was used to guide the 3D geostatistical modeling of rock types. This was conducted by using normalized trend (probability) maps and volumes for each rock type based on the ranges of p-impedance values associated with rock types. A linear gradient was applied to areas between high and low probability. Additionally, the p-impedance and ϕ_t cross-plot had a negative relationship. When filtered by rock type, relative trends of high and low ϕ_t were observed for each rock type.

3D Reservoir Modeling

3D reservoir models of the Wolfcamp Formation were built to map and evaluate the spatial distribution and stratigraphic variability of rock types and associated petrophysical and geomechanical properties. The areal grid dimensions were determined based on, in part, the average distance between wells, and the vertical resolution was set to preserve the stratigraphic

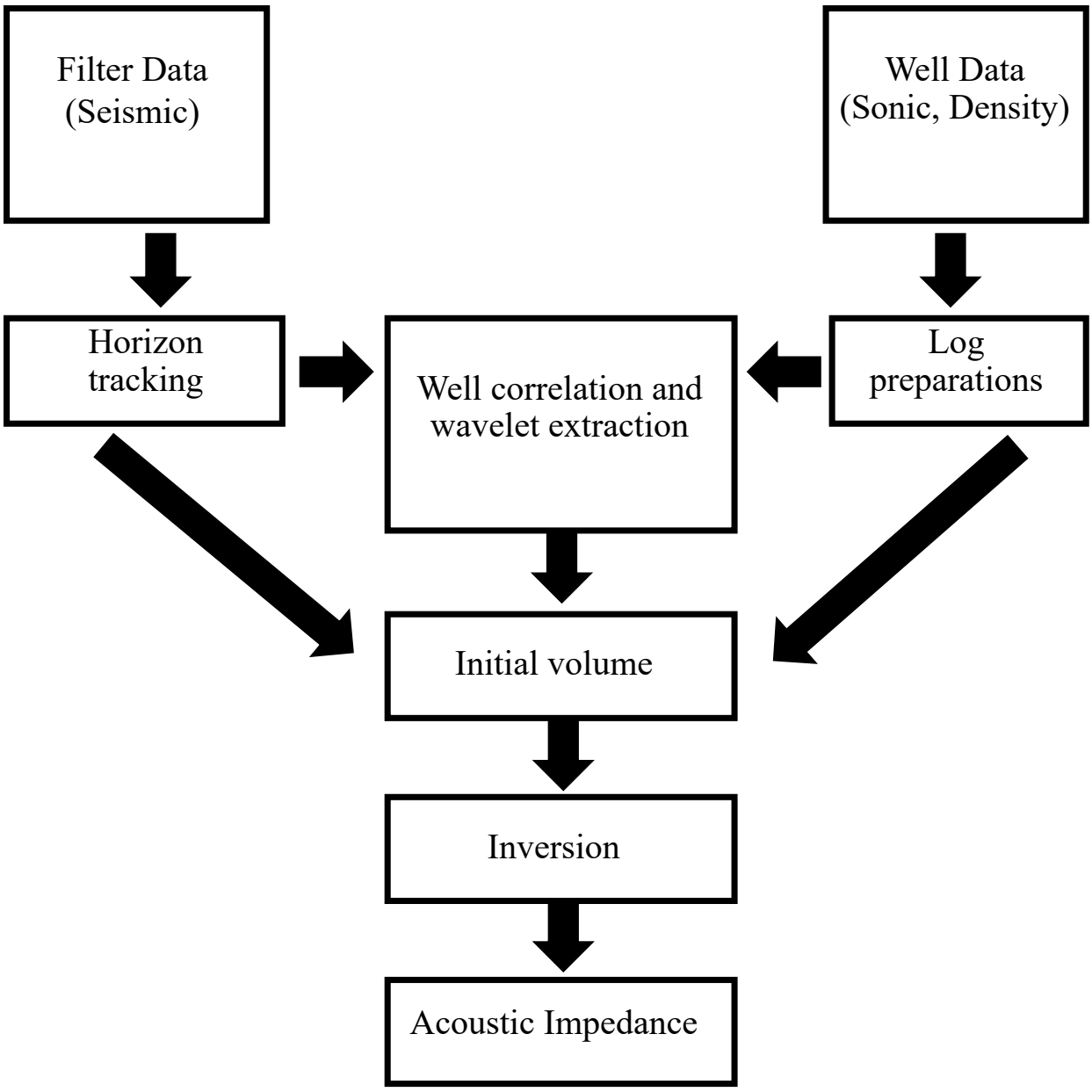


Figure 6: Generalized post-stack seismic inversion workflow (Farfour et al., 2015). The seismic horizons, well logs (Sonic and RHOB), and well-top data were used to perform seismic-to-well ties which define a time-depth relationship (TDR) allowing a wavelet phase to be extracted. An initial p-impedance background volume is created and the results are analyzed by comparing the synthetic trace to the actual seismic trace. Once the error is reduced by manually adjusting the wavelet phase, the final inversion model is established.

variability of rock types while maintaining a reasonable number of cells in the grid. The Wolfcamp Formation structure-contour maps were used to define 4 model zones (A-D). Within each zone, proportional layering was used for the stratal geometry. The number of layers for each zone was determined by dividing the average thickness of each Zone by the vertical cell height.

Rock-type, petrophysical, and geomechanical logs were upscaled to the resolution of the 3D grid. The rock-type logs were upscaled first, and the subsequent petrophysical and geomechanical logs upscaled biased to the rock-type logs. The accuracy of the upscaling was validated by comparing the original and upscaled logs with frequency histograms (for rock-type proportions) and cross sections (for rock-type presence).

Two rock type models were made using average p-impedance trend maps or p-impedance trend volumes for each rock type. The rock type models were stochastically modeled using sequential-indicator-simulation (SIS) constrained to the (1) stratigraphic framework (3D grid), (2) upscaled rock-type logs, (3) rock-type percentages by zone, (4) vertical rock-type proportion curves, (5) vertical and horizontal variogram parameters by rock type and zone, and (6) p-impedance trend maps or volumes for each rock type. Assuming the geometry of debris flows in the Wolfcamp Formation are relatively thin sheet-like deposits, the range for major and minor directions of horizontal variogram parameters were set assuming no preferential direction of anisotropy. Multiple rock-type vertical proportion curves were tested within the area to more fully account for potential lateral variations of rock types. However, the limited distribution of wells with rock-type logs did not allow the area to be subdivided for the use of multiple vertical rock-type proportion curves. For that reason, the rock-type model was constrained to a single vertical proportion curve. Thirty realizations of each model were computed to capture the range

uncertainty in rock types and associated ϕ_e, S_w, pore volume, and HCPV. The P10 (most conservative), P50 (middle), and P90 (most optimistic) cases were determined and models for the P50 cases are presented.

The V_{sh}, ϕ_t, S_w, and BI models were constrained to the (1) stratigraphic framework (3D grid), (2) their respective upscaled logs, (3) rock-types, (4) calculated vertical and horizontal variograms, and (5) histograms for each property. The modeling method used was sequential-Gaussian-simulation (SGS). The vertical and horizontal variograms major and minor ranges were less than the rock-type variogram ranges given the property variability within each rock type. The range for major and minor directions of horizontal variograms was set assuming no preferential direction of anisotropy, similarly to the rock-type model.

The ϕ_e model was calculated from the ϕ_t and V_{sh} models. This was done to constrain the ϕ_e model directly to those models. The ϕ_e model was calculated by subtracting the mudstone pore volume from the ϕ_t (Equation 4). The mudstone rock type was set to 0.0% for ϕ_e.

RESULTS

Petrophysical and Geomechanical Properties, Mineralogy, and Rock Types

V_{sh} was calculated using the Stieber equation (Thomas and Stieber, 1975) to avoid misinterpretation observed when V_{sh} is calculated using gamma-ray alone. The Stieber equation (Equation 1) is based on an empirical relationship that is more reliable and applied for rocks deposited for the geologic age of the Wolfcamp Formation (Bassiouni, 1994). An assumed simplistic linear relationship between high gamma-ray values and the presence of mudstone often leads to an over-estimation of V_{sh} (Thomas and Stieber, 1975; Bassiouni, 1994). The over-estimation occurs because this method assumes all radioactive minerals are associated with

mudstone. However, this becomes an issue when uranium and other non-sedimentary rock forming mineral are present. For the Wolfcamp in the study area, V_{sh} ranges from 0-100% with an average ~30% (Figure 3). Higher values of V_{sh} are common in the lower and middle Wolfcamp Formation.

ϕ_t and ϕ_e (Equation 3 and 4) for the entire Wolfcamp Formation both range from 0-16%, and average ~10% and 4%, respectively. Both ϕ_t and ϕ_e vary stratigraphically and general are higher in dolomites and lower in limestones (Figure 3). The average S_w (Equation 5) for the entire Wolfcamp Formation is 35% and ranges from 0 to 100%. The stratigraphic distribution of S_w increases moving stratigraphically upward. Lower values of S_w generally correspond to mudstone and high values vary between limestones and sandstones (Figure 3). BI is relative to each case study. The entire Wolfcamp Formation shows a relative high proportion of brittle rock with BI ranging from 0-0.97 with an average 0.64. The stratigraphic distribution of BI is highly variable. Lower BI values correlate to limestones and mudstone and higher BI values correlate to sandstones and dolomites (Figure 3).

Based on ρ_{maa}-U_{maa} analysis, the Wolfcamp Formation has 29% mudstone, 27% limestone, 22% sandstone, and 22% dolomite (Figure 3). The stratigraphic distribution of rock types reflects the variability in mineral composition throughout the Wolfcamp Formation. The base of the Wolfcamp is primarily composed of mudstone and decreases moving upward through the section. Dolomite and limestone proportions are limited at the base of the interval and increase as mudstone decreases however before they reach the top of the section they both begin to decrease. Sandstone percent is low in lower and middle Wolfcamp and is dominant in the upper Wolfcamp.

Stratigraphic and Structural Framework

The Wolfcamp Formation (top Wolfcamp) gradually dips to the east-southeast or basinward and varies in elevation from -4764 to -5600 ft (-1454 to -1706 m). Based on well-log signatures and seismic response, the Wolfcamp Formation is divided into 4 operational units, from top to bottom, Zones A-D (top Wolfcamp represents the top of Zone A; top Cisco represents the base of the Wolfcamp interval) and are laterally continuous throughout the study area. West-east inlines from the seismic volume illustrate the depositional dip of the Wolfcamp Formation and the proximal-to-distal variation in thickness (Figure 7). Structural cross-sections (Figure 8) and isopach maps illustrate the structural and stratigraphic variability of Wolfcamp operational units. The depositional dip and thickness variation of the Wolfcamp are results of high frequency changes in sea level and mild tectonic activity that influenced major developmental factors of the reef margin and initiated deep-seated faults associated with differential subsidence (Hurst and Surlyk, 1984; Mazzullo, 1984; Hobson et al., 1985; Shumaker, 1992). Structure-contour maps show that the Wolfcamp is structurally high in the north-northwest and gradually deepens to the east-southeast (Figure 9). Isopach maps illustrate that the Wolfcamp Formation ranges in thickness from 500 to 1200 ft (152 to 365 m) and becomes thicker to the east-southeast in the distal region of the study area. The range in thickness varies in Zone A from 129-500 ft (39-152.4 m); Zone B from 171-508 (52-154.8 m); Zone C from 67-395 ft (20.4-m120.3); and Zone D from 78-323 ft (23.7-98.4 m). The average thickness of each Zone ranges from 227-508 ft (69-154.8 m) and all zones thicken to the east-southeast (Figures 9 and 10).

P-Impendance, Rock Types, and Porosity Trends

Ranges in well-log p-impedance values approximately correspond to different rock types with moderate overlap. Mudstones have relatively low values, sandstones and dolomites have

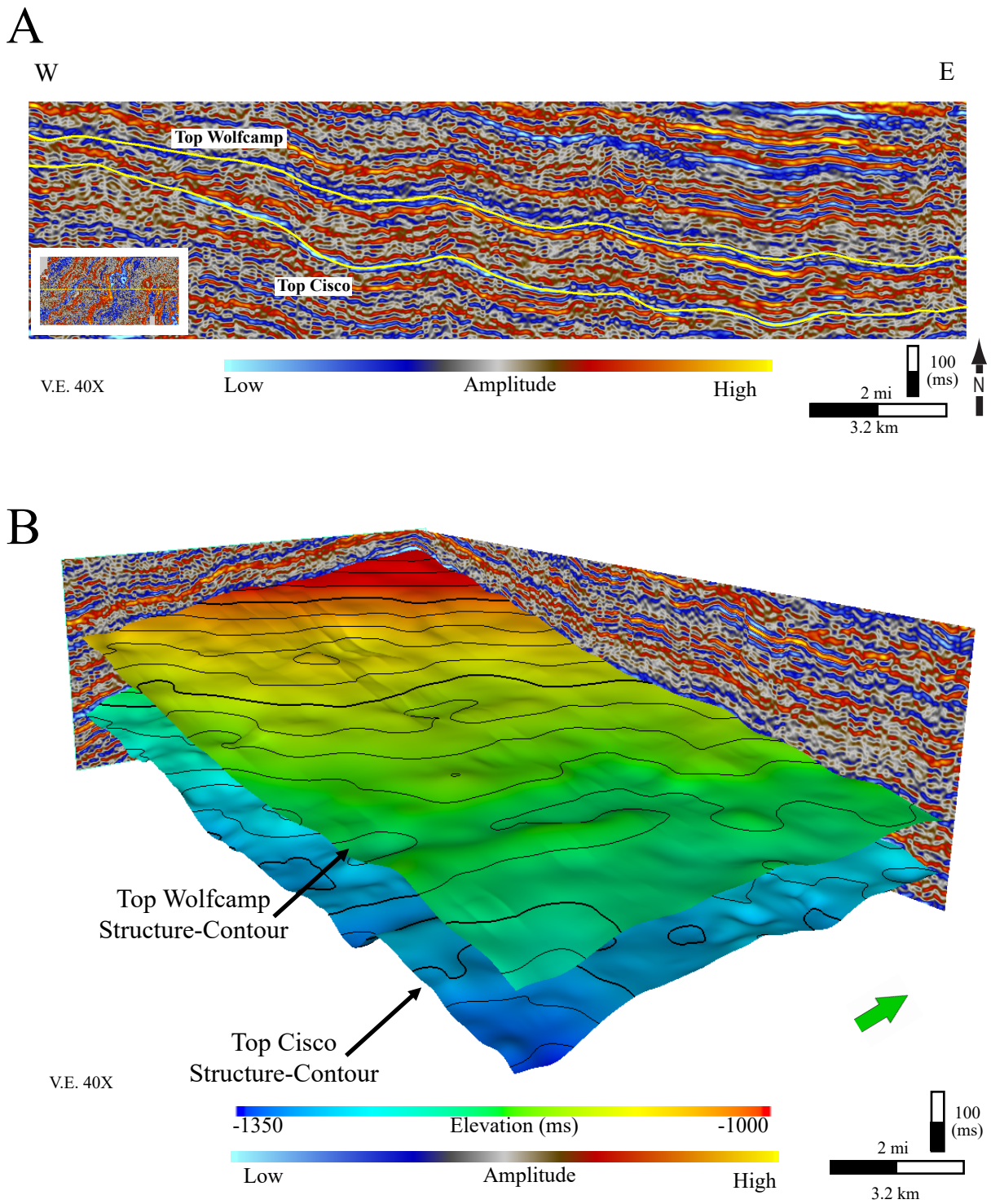


Figure 7: A) West-east oriented seismic inline displays the horizon tops for the Wolfcamp and Cisco (base Wolfcamp) Formations were picked on low amplitude reflectors. B) The seismic amplitude volume and top Wolfcamp and Cisco mapped surfaces illustrate the east-southeast depositional dip and proximal-to-distal spatial variation in thickness within the study area.

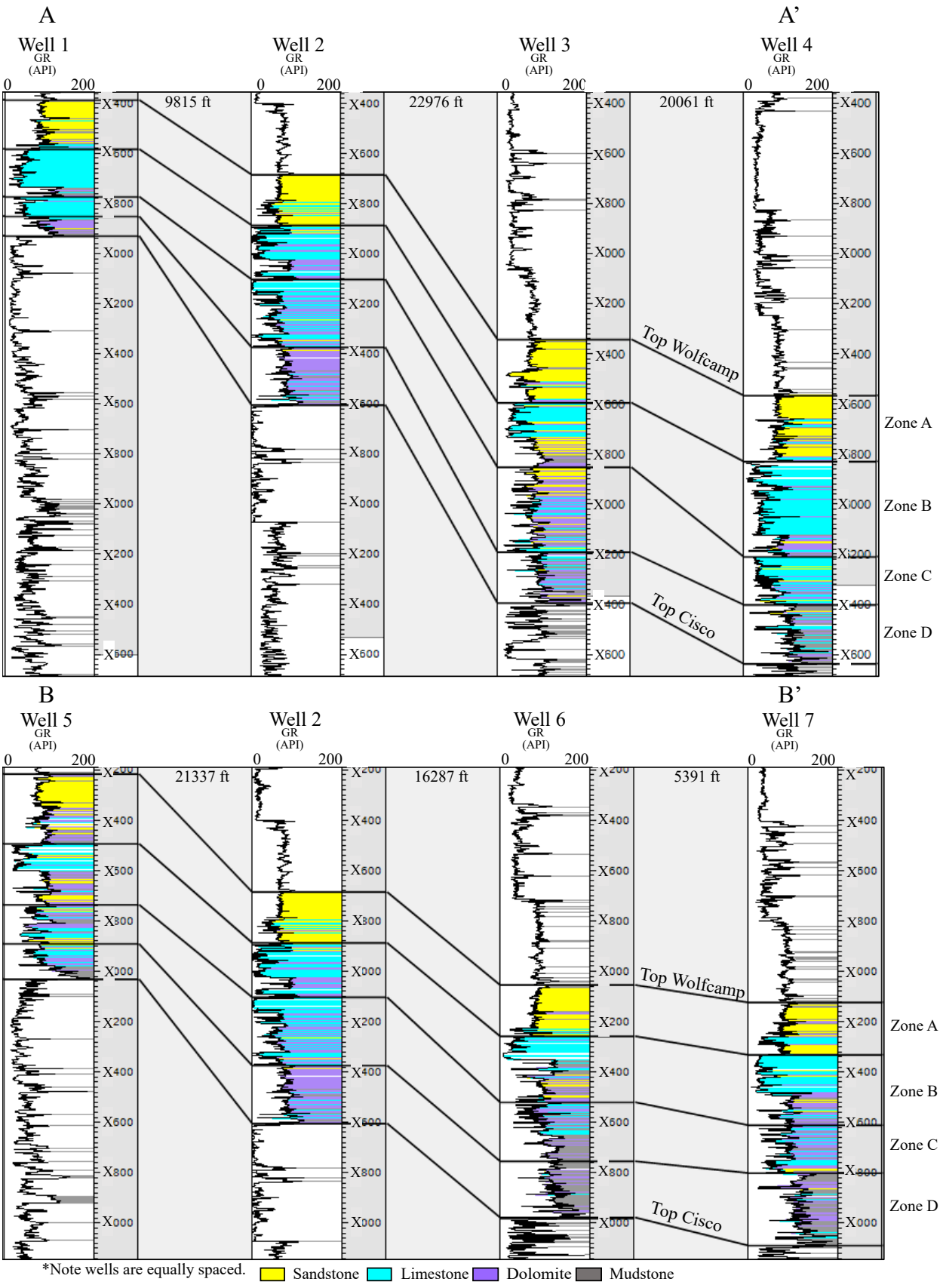

A
A'
Well 1
Well 2
Well 3
Well 4
GR
(API)
0
200
9815 ft
22976 ft
20061 ft
Top Wolfcamp
Top Cisco
Zone A
Zone B
Zone C
Zone D
B
B'
Well 5
Well 2
Well 6
Well 7
21337 ft
16287 ft
5391 ft
*Note wells are equally spaced.
Sandstone
Limestone
Dolomite
Mudstone

Figure 8: A-A' is a west-east oriented structural cross-section illustrating the structural dip, stratigraphic variation in rock type, and Zone thickness. B-B' is a southwest-northeast structural cross section illustrating less variation in zone thickness. This is consistent with structure-contour and isopach maps that show zones thicken proportionately in the direction of depositional dip. Location of cross-sections are shown in Figure 1. *Note that well are equally spaced.

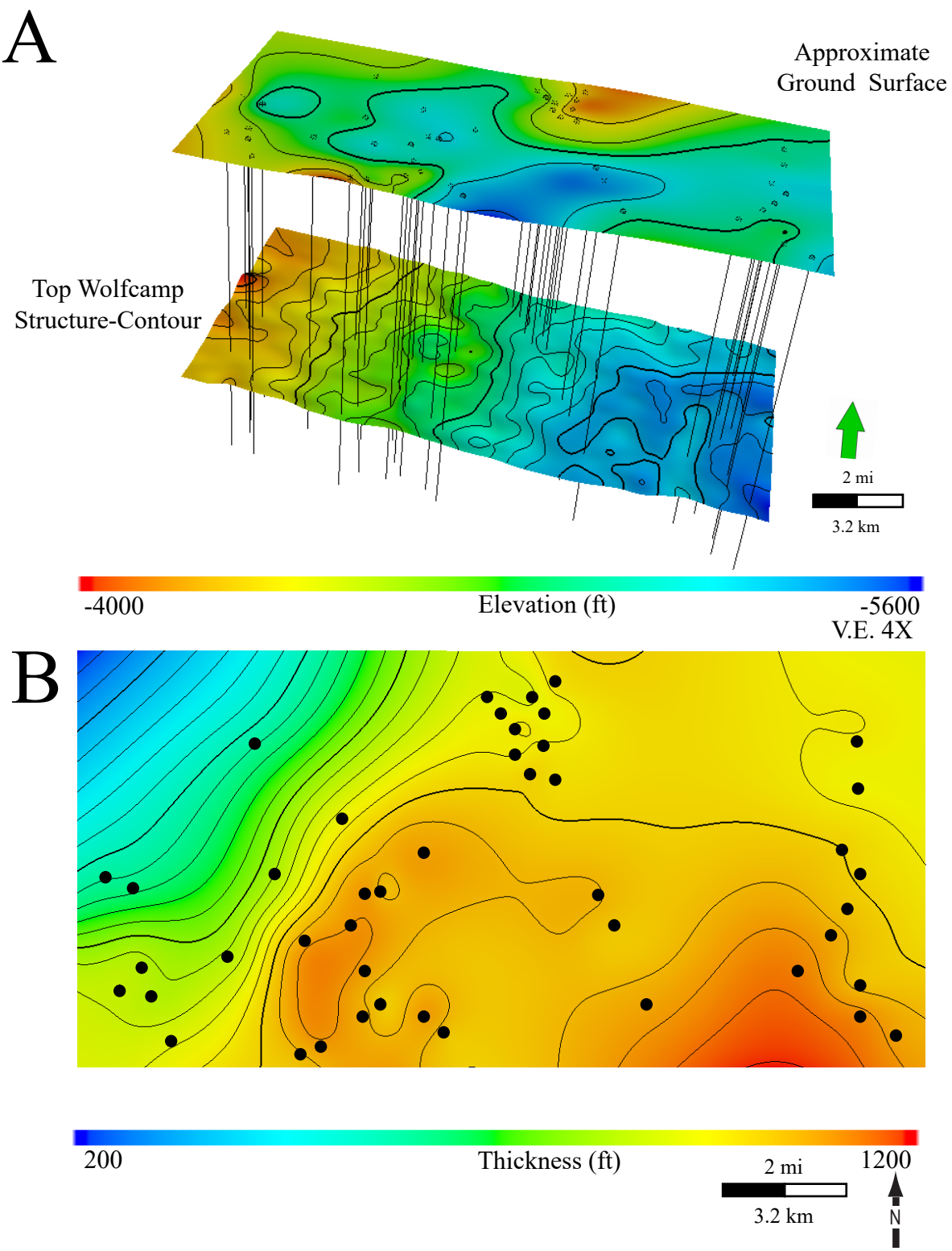


Figure 9: A) The top Wolfcamp structure-contour map and location of the wells within the study area. Map displays the gradual dip to the east-southeast. B) The Wolfcamp interval isopach map and the location of the wells within the study area. The Wolfcamp becomes more thick to the east-southeast reaching its maximum thickness ~1200 ft (365 m).

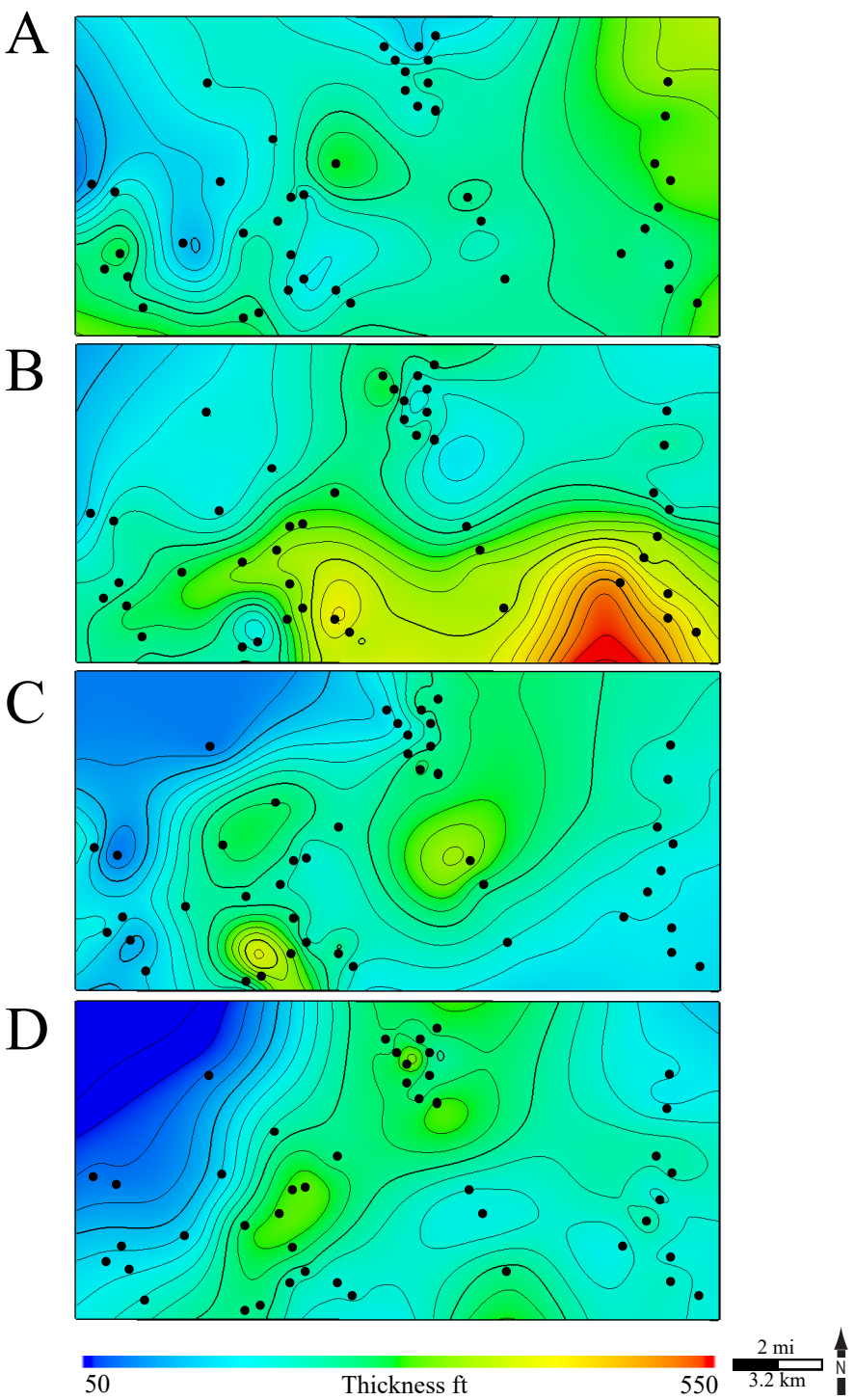


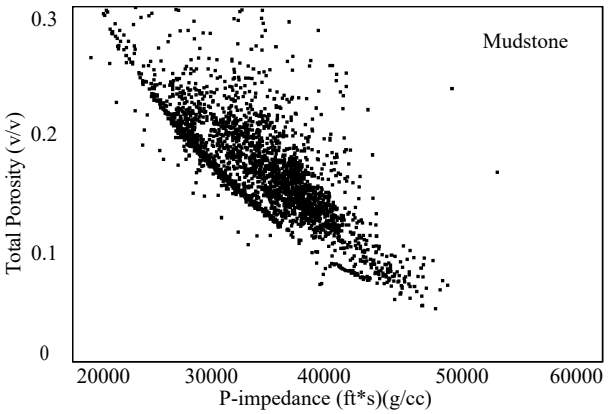
Figure 10: Isopach maps and well locations for A) Zone A, B) Zone B, C) Zone C, and D) Zone D illustrate proportional thickening to the east-southeast. The range in thickness varies in Zone A from 129-500 ft (39-152.4 m); Zone B from 171-508 (52-154.8 m); Zone C from 67-395 ft (20.4-120.3 m); and Zone D from 78-323 ft (23.7-98.4 m).

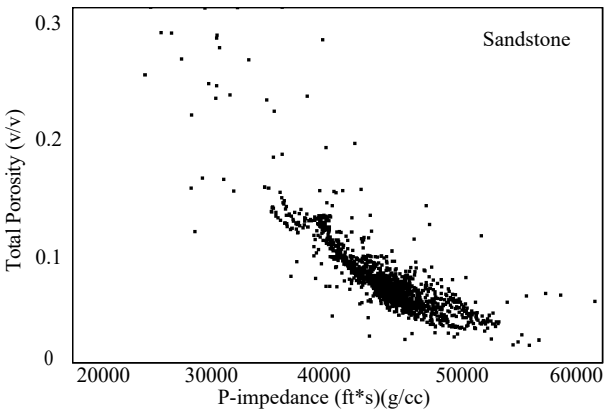
intermediate values, and limestones have relatively high values of p-impedance. Approximate log-based p-impedance values for each rock type are: mudstones from 20,000-40,000 (ft*s)(g/cc); sandstones from 40,000-50,000 (ft*s)(g/cc); limestones from 48,000-68,000 (ft*s)(g/cc); and dolomites from 32,000-48,000 (ft*s)(g/cc) (Figure 11).

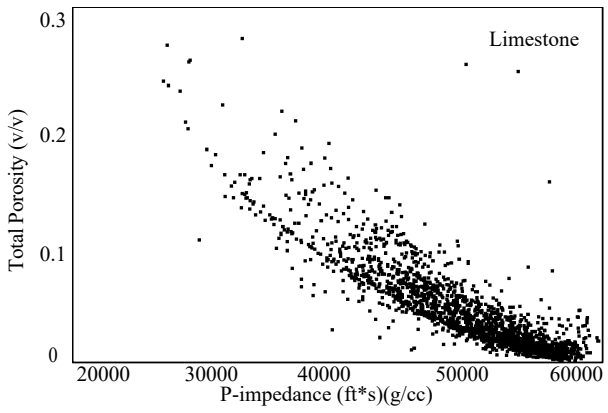
An average error between the well-log calculated p-impedance and the inversion p-impedance is 0.39, mostly occurring in the lower Wolfcamp and above the interval of interest (Figure 12). Based on the seismic inversion, values of p-impedance range from 0-68,700 (ft*s)(g/cc). Average p-impedance for the Wolfcamp Formation derived from the inversion volume ranges from 35,000-50,000 (ft*s)(g/cc). Spatially, higher p-impedance values occur in the northwest portion of the study area (Figure 13A).

Using the average p-impedance map and the depth converted p-impedance volume for the Wolfcamp Formation, the spatial distribution for each rock type was guided by their respective ranges in p-impedance values. The spatial distributions for mudstone and limestone are more distinct than sandstone and dolomite. Limestone is dominant in the northwestern portion of the study area and mudstone increases to the east-southeast. Dolomite and sandstone generally have less distinct trends with an exception in the northwest in which both rock types are less common. Mudstone, sandstone, and dolomite are less abundant in the northwest which corresponds to a structurally higher area with relatively thin zones and higher p-impedance values (Figure 13) (Appendix E).

The negative relationship between total porosity (ϕ_t) and p-impedance (Z_p) illustrates that high ϕ_t corresponds to low p-impedance. Given the relationship among ϕ_t, rock-types, and p-impedance values, areas of low p-impedance have greater proportions of mudstone, sandstone,


Mudstone
Total Porosity (v/v)
0.3
0.2
0.1
0
20000
30000
40000
50000
60000
P-impedance (ft*s)(g/cc)


Sandstone
Total Porosity (v/v)
0.3
0.2
0.1
0
20000
30000
40000
50000
60000
P-impedance (ft*s)(g/cc)


Limestone
Total Porosity (v/v)
0.3
0.2
0.1
0
20000
30000
40000
50000
60000
P-impedance (ft*s)(g/cc)

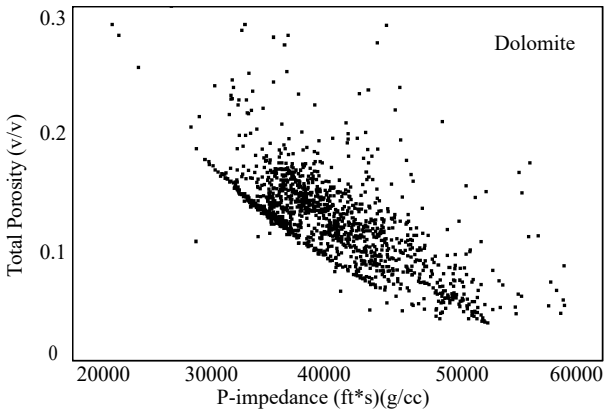

Dolomite
Total Porosity (v/v)
0.3
0.2
0.1
0
20000
30000
40000
50000
60000
P-impedance (ft*s)(g/cc)

Figure 11: Total porosity and well-log p-impedance cross-plots for A) mudstone, B) sandstone C) limestone and D) dolomite identify specific range of p-impedance values for each rock-type; mudstone 28,000-40,000 (ft*s)(g/cc), sandstone 40,000-50,000(ft*s)(g/cc), limestone 48,000-68,000(ft*s)(g/cc), and dolomite 32,000-48,000(ft*s)(g/cc). The relationship established between well-log p-impedance and rock types suggested use of inversion derived p-impedance to spatial distribute rock types within the study area.

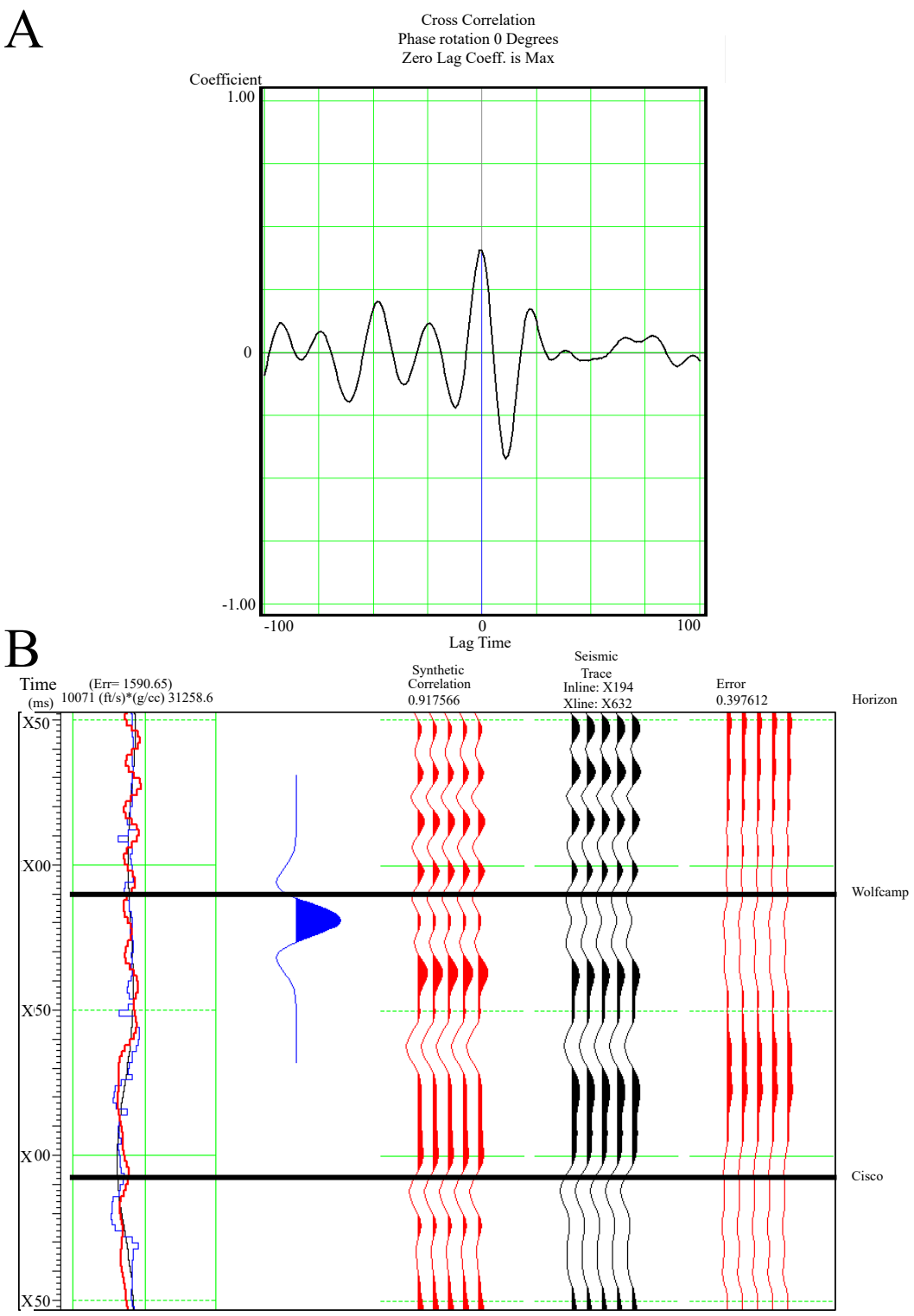


Figure 12: (A) The cross-correlation of an extracted statistical wavelet from one of the wells in the volume. (B) The results of the inversion volume. The first track shows p-impedance computed from well logs (blue) and the inversion p-impedance (red). The error between the two is 0.397 mostly occurring in the base Wolfcamp and above the interval.

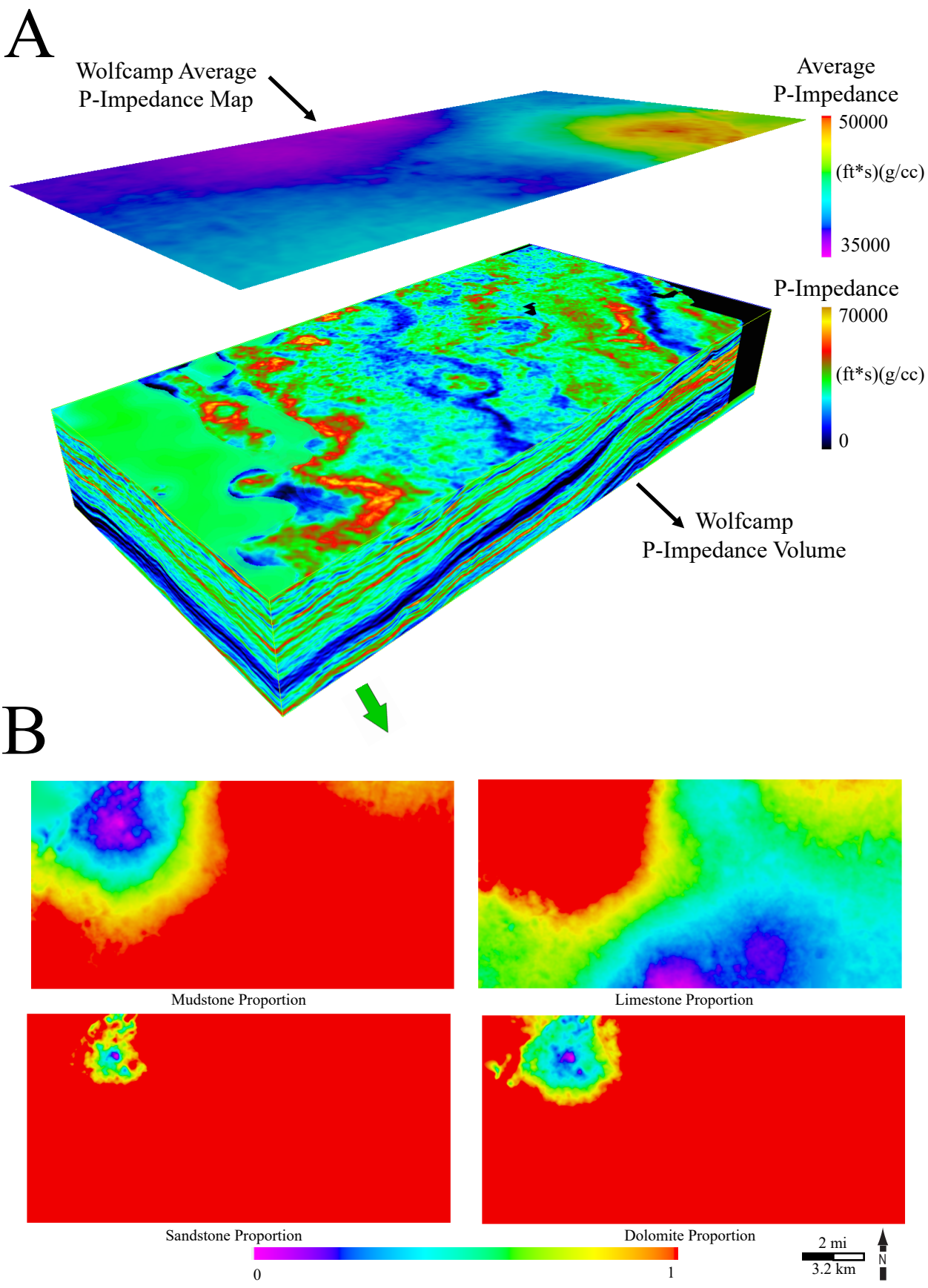

A
Wolfcamp Average
P-Impedance Map
Average
P-Impedance
50000
(ft*s)(g/cc)
35000
P-Impedance
70000
(ft*s)(g/cc)
0
Wolfcamp
P-Impedance Volume
B
Mudstone Proportion
Limestone Proportion
Sandstone Proportion
Dolomite Proportion
0
1
2 mi
3.2 km
N

Figure 13: A) The average p-impedance map derived from the p-impedance inversion was used to map the rock types based on their corresponding range of p-impedance values. The spatial trend maps B) mudstone, C) sandstone, D) limestone, and E) dolomite were normalized and rescaled in such a way that 1 represents a high probabilty of specified rock type distribution and 0 indicates a low probability of specified rock type distribution. A gradational trend was applied between areas of high and low probability. The mudstone and limestone maps display distinct trends in distribution while sandstone and dolomite do not with the exception of the northwest portion of the study area.

and dolomite and higher ϕ_t values. Areas of high p-impedance are associated with limestone and lower ϕ_t values.

Spatial Distribution of Rock Types, Petrophysical and Geomechanical Properties

For the Wolfcamp Formation, thirty rock-type and petrophysical and geomechanical realizations were generated as well as their associated pore volume and hydrocarbon pore volume (HCPV) to evaluate the spatial variability and range of uncertainty of these properties. Rock type, ϕ_e, S_w, and BI were modeled within the Wolfcamp stratigraphic framework as represented by a three-dimensional reservoir model grid that contain cells with dimensions of 200 X 200 ft (60 X 60 m) areally (I and J directions) and ~2 ft (~0.6 m) vertically (K direction). The 3D grid has 29,434,581 cells (Figure 14).

For the rock-type models (map-based and volume-based), for all rock types, vertical variogram ranges were estimated to be ~20 ft (~6 m) and horizontal variograms are set to 10,000 (3,048 m) for the major and minor directions. For petrophysical and geomechanical models, vertical variogram ranges are 7-15 ft (2-4.5 m) and horizontal variogram ranges are set to 8,000 (2,438 m) for the major and minor directions.

In terms of the rock type distribution, the trend maps for limestone and mudstone show distinct trends that are reflected in the spatial distribution of these rock types (Figure 15). Each stratigraphic zone has a dominant mineralogy and rock-type composition; e.g., Zone A (quartz, sandstone), Zone B (calcite, limestone), Zone C (dolomite), and Zone D (clay, mudstone) (Figures 3 and 16). The lithology at the base of the Wolfcamp is dominantly mudstone in Zone D. Moving stratigraphically upward through the Wolfcamp, the lithologies becomes more carbonate-rich (limestones and dolomites) in Zones C and B. In Zone A, the lithology composition transitions from carbonate-rich to primarily sandstones (Figures 3 and 16).

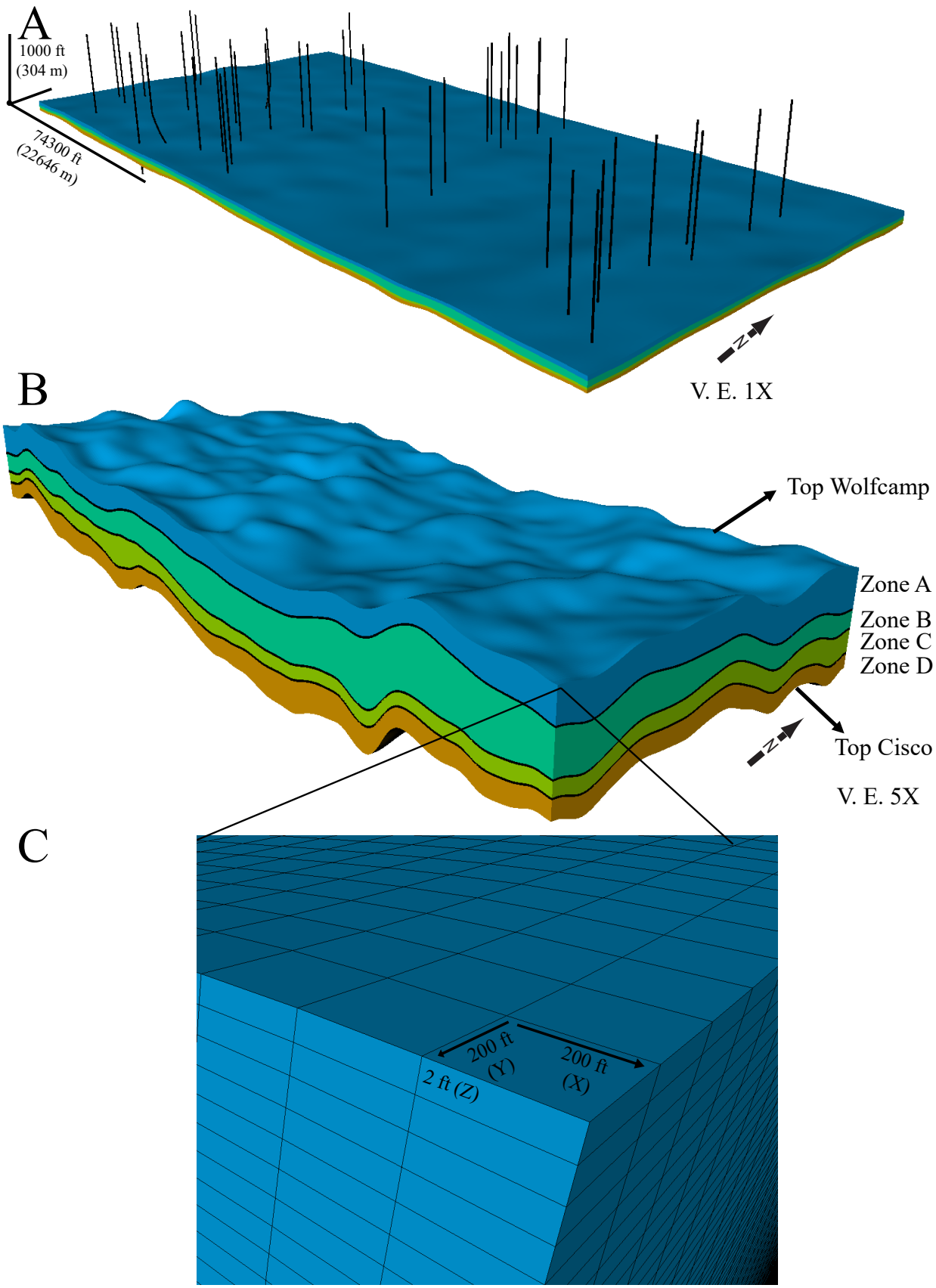

A
1000 ft
(304 m)
74300 ft
(22646 m)
Z
V. E. 1X
B
Top Wolfcamp
Zone A
Zone B
Zone C
Zone D
Top Cisco
Z
V. E. 5X
C
200 ft
(Y)
200 ft
(X)
2 ft (Z)

Figure 14: A) The interpreted stratigraphic Zones of the Wolfcamp Formation within the study area with areal dimension of 74300 ft (~22,646 m) X 35752 ft (~10,897 m) and ~ 1000 ft (304 m) thick. B) A 3D reservoir model grid of the Wolfcamp Formation was built to model and evaluate the spatial distribution and stratigraphic variability of rock types and associated petrophysical and geomechanical properties. The Wolfcamp Formation structure-contour maps were used to define 4 model Zones (A-D). Within each Zone, proportional layering was used for the stratal geometry. The number of layers for each zone was determined by dividing the average thickness of each Zone by the vertical cell height. C) The areal grid dimensions were determined based on, in part, the average distance between wells, and the vertical resolution was set to preserve the stratigraphic variability of rock types while maintaining a reasonable number of cells in the grid. The 3D reservoir model grid contains cells with dimensions of 200 X 200 ft (60 X 60 m) areal (I and J directions), ~2 ft (~0.6 m) vertically (K direction), with a total of 29,434,581 cells.

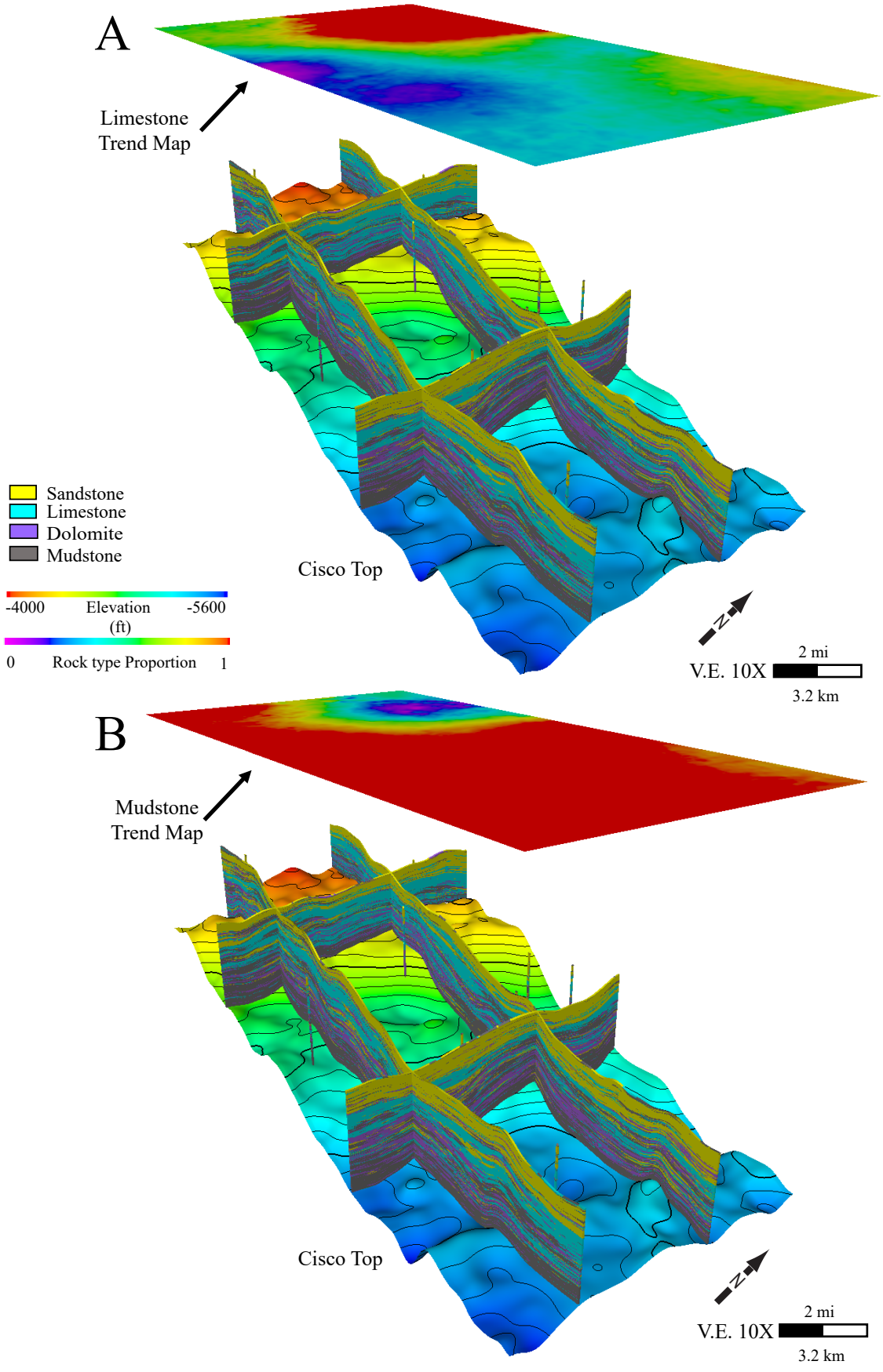

A
Limestone
Trend Map
Sandstone
Limestone
Dolomite
Mudstone
-4000
Elevation
(ft)
-5600
0
Rock type Proportion
1
Cisco Top
N
2 mi
V.E. 10X
3.2 km
B
Mudstone
Trend Map
Cisco Top
N
2 mi
V.E. 10X
3.2 km

Figure 15: North-south and west-east profiles through the rock-type model reflect the distinct distribution trends observed in the A) limestone and B) mudstone trend maps. Limestone shows more distribution in the northwest portion of the study area while mudstone shows limited distribution in the northwest and increases to the east-southeast.

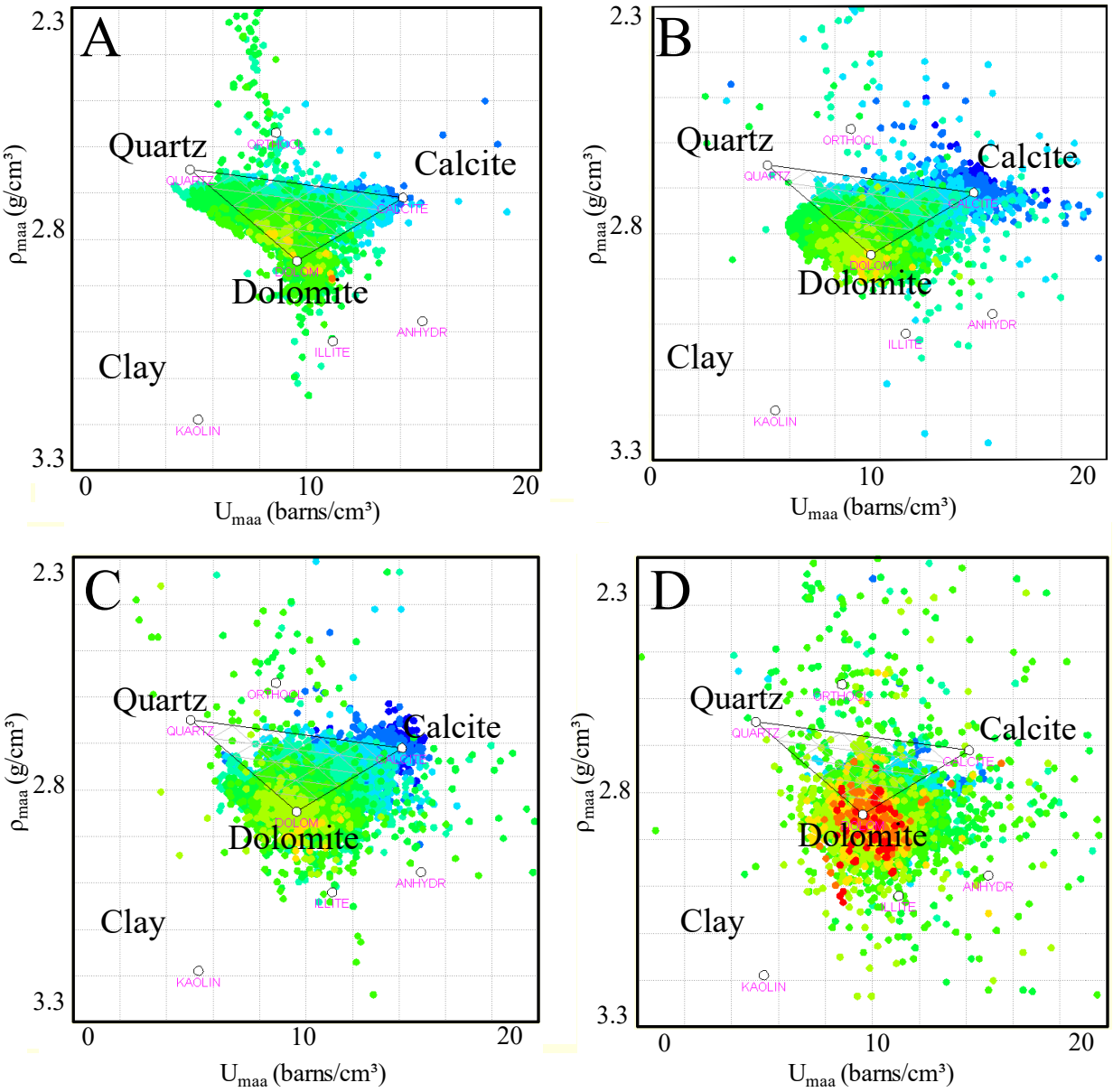


Figure 16: The ρmaa-Umaa analysis per Zone illustrates the stratigraphic variability of mineral composition for A) Zone A, B) Zone B, C) Zone C and D) Zone D. Each stratigraphic zone has a dominant mineralogy and rock-type composition; e.g., Zone A (quartz, sandstone), Zone B (calcite, limestone), Zone C (dolomite), and Zone D (clay, mudstone) The lithology at the base of the Wolfcamp is dominantly mudstone in Zone D. Moving stratigraphically upward through the Wolfcamp, the lithologies becomes more carbonate-rich (limestones and dolomites) in Zones C and B. In Zone A, the lithology composition transitions from carbonate-rich to primarily sandstones. The dominant mineral composition of each zone is reflected in the rock-type vertical proportion curve (Figure 3).

Limestone percent increases upward through the Wolfcamp (mean percentages of 7%, 33%, 52% from Zones D, C, and B, respectively) (Figure 17).

Zone C has the highest ϕ_e with a range of 1 to 12% and an average of 6%. Higher ϕ_e within Zone C is observed in dolomite and low ϕ_e is associated with limestone (Figures 18 and 19). This observation is consistent with the higher range in p-impedance for limestone (48,000-68,000 (ft*s)(g/cc)) and lower values associated with dolomite (32,000-48,000 (ft*s)(g/cc)) (Figure 11). ϕ_e is lowest for Zone D and ranges from 0 to 12% with a mean of 3.5%. The lower values are associated with the larger proportion of mudstone in Zone D. Zones A-C show an upward decrease in mean ϕ_e from 5.8% to 4.3% to 3.9%.

The average S_w for the entire Wolfcamp interval is 35% and S_w ranges from 0 to 100%. Mean S_w shows an upward increase in the Wolfcamp Formation from 16% in Zone D, 32% in Zone C, 36% in Zone B, to 48% in Zone A, with Zone A being primarily composed of sandstone (Figures 18 and 19).

BI ranges from 0-0.97 with a mean of 0.67. By zone, mean BI varies from 0.76 in Zone A, 0.52 in Zone B, 0.65 in Zone C, and 0.66 in Zone D. This reflects the dominate mineralogy and rock type for each zone (Figures 18 and 19). The zone with the lowest BI (Zone B) is largely composed of limestone while the zones with higher BI (especially Zones A and C) are primarily composed of sandstone and dolomite, respectively. Moderate ranges of BI are favorable for drilling environment, hole integrity and hydraulic fracturing.

Pore volume and hydrocarbon pore volume increase moving stratigraphically upward through the Wolfcamp Formation. Dolomite has highest pore volume and HCPV but is least represented in terms of bulk volume within the Wolfcamp (Table 1). Relatively poor reservoir

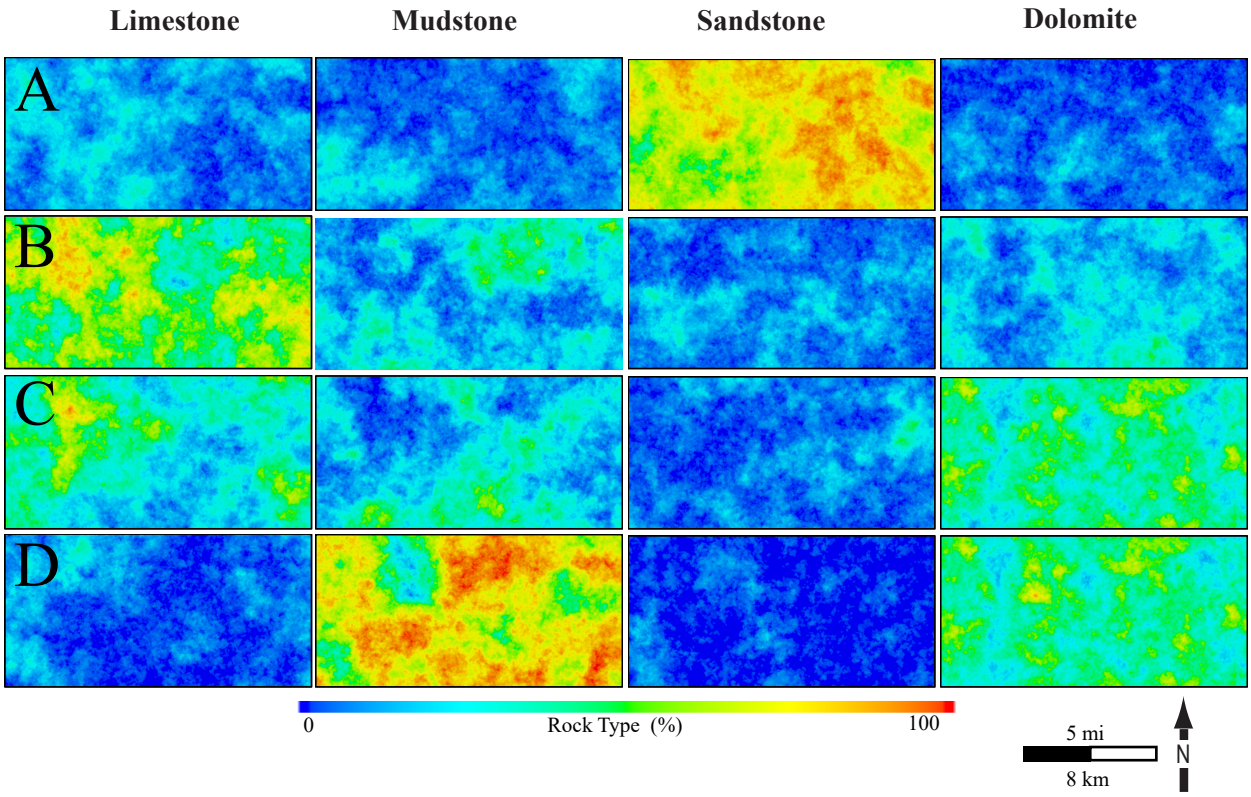


Figure 17: The spatial distribution of rock types and associated reservoir quality are illustrated by the percentage of each type in A) Zone A, B) Zone B, C) Zone C, and D) Zone D. Zone A and B are primarily composed of sandstone and mudstone, which both exhibit over all poor reservoir quality in terms of Φ_e, BI, and S_w. Zone B-D illustrate an upward increase of limestone.

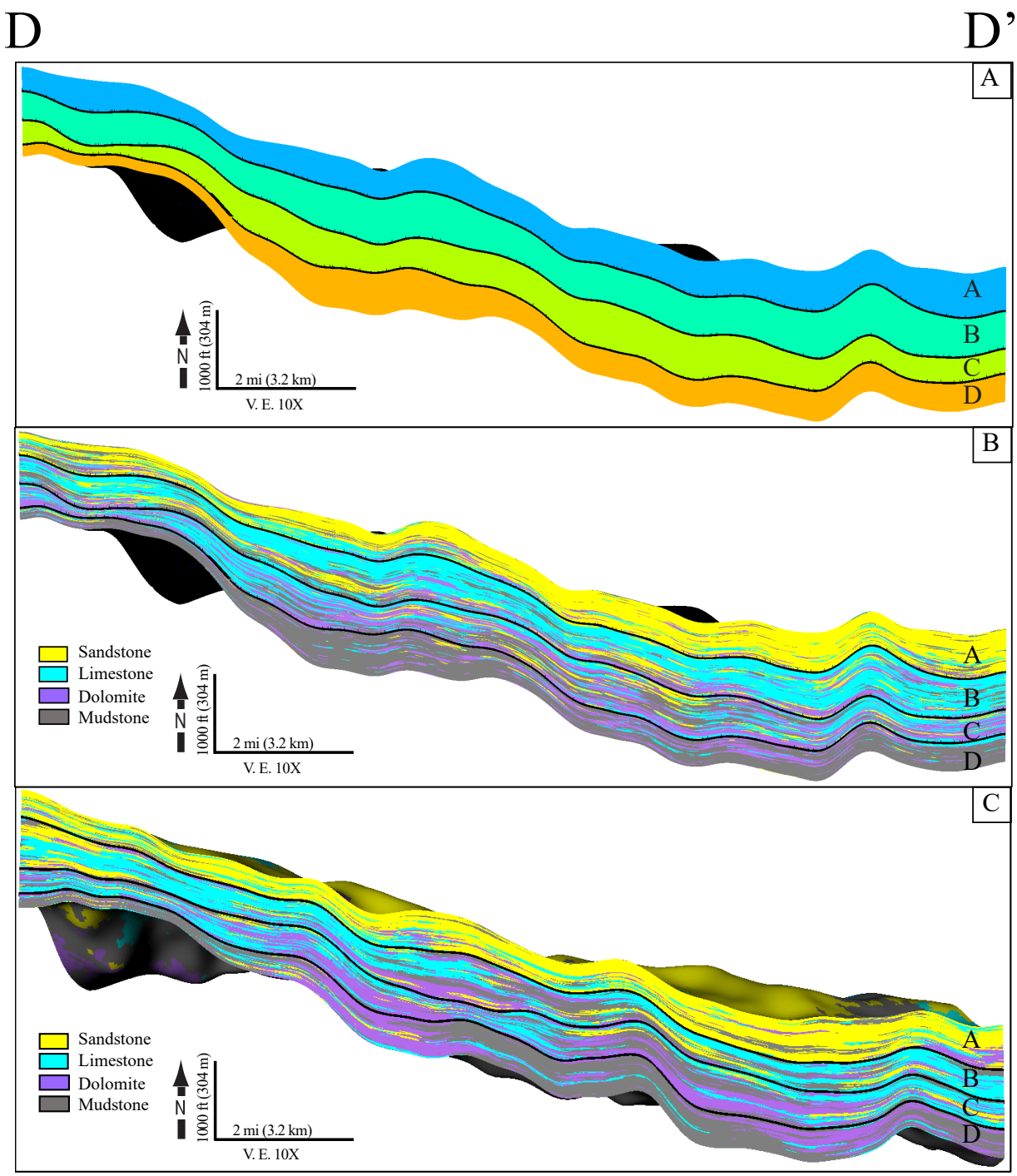

D
D’
A
A
B
C
D
N
1000 ft (304 m)
2 mi (3.2 km)
V. E. 10X
B
Sandstone
Limestone
Dolomite
Mudstone
A
B
C
D
N
1000 ft (304 m)
2 mi (3.2 km)
V. E. 10X
C
Sandstone
Limestone
Dolomite
Mudstone
A
B
C
D
N
1000 ft (304 m)
2 mi (3.2 km)
V. E. 10X

Figure 18: West-east orientated profiles through the 3D model A) illustrate the stratigraphic Zones and their variation in thickness, B) illustrate the spatial distribution in rock types modeled by average p-impedance trend maps and, C) illustrate the spatial distribution in rock types modeled by p-impedance trend volumes of the Wolfcamp Formation. The base of the Wolfcamp is primarily composed of mudstone and decreases moving upward through the section. Dolomite and limestone proportions are limited at the base of the interval and increase as mudstone decreases however before they reach the top of the section they both begin to decrease. Sandstone shows little to no distribution at the base of the interval and increases as mudstone, limestone, and dolomite began decreasing toward the top of the section. The top of the section is nearly all composed of sandstone. The Wolfcamp Formation has 29% mudstone, 27% limestone, 22% sandstone, and 22% dolomite (Figure 3). The models shown represent the P50 realization based on uncertainty analysis discussed in the Spatial Distribution of Rock types, Petrophysical and Geomechanical Properties sections.

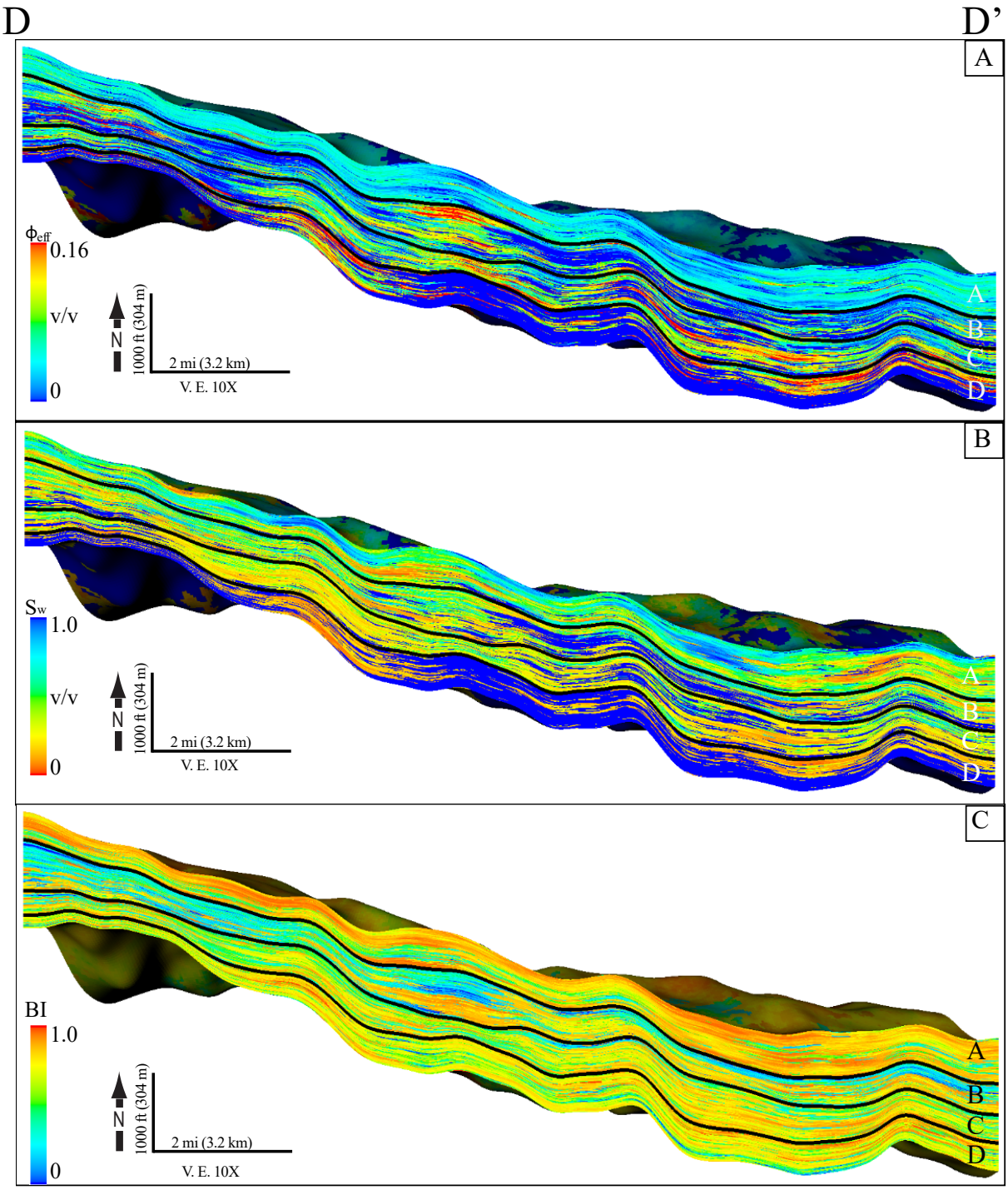

D
D'
A
ϕ_{eff}
0.16
v/v
0
N
1000 ft (304 m)
2 mi (3.2 km)
V. E. 10X
A
B
C
D
B
S_w
1.0
v/v
0
N
1000 ft (304 m)
2 mi (3.2 km)
V. E. 10X
A
B
C
D
C
BI
1.0
0
N
1000 ft (304 m)
2 mi (3.2 km)
V. E. 10X
A
B
C
D

Figure 19: West-east oriented profiles through the 3D models A) illustrate the spatial distribution of Φ_e within the study area. Φ_e is highly variable but generally increases in dolomites and decreases in limestones (Figure 18). Highest Φ_e values are located distal from the north-northwest within Zone B and C (mean= 4.3%, 5.8%, respectively). B) Illustrates the spatial distribution of S_w within the study area. Generally moving up section Zone A-D increases in S_w (means= 48%, 36%, 32%, 16%, respectively). C) Illustrates the spatial distribution of BI within the study area. Moving up section, Zones C and D show high BI (mean= 0.65, 0.66, respectively). Zone B displays the lowest value in BI and Zone A contains the highest value of BI (mean= 0.52, 0.76, respectively). Low values of BI correspond to limestones and mudstones while high values correspond to sandstones and dolomites (Figure 17).

	Bulk Volume ($*10^9$ RB)	Pore Volume ($*10^9$ RB)	Hydrocarbon Pore Volume ($*10^9$ RB)
Zone A	116	4.5	2.3
Mudstone	9.9	0	0
Sandstone	85.4	3.6	1.6
Limestone	14.2	0.6	0.4
Dolomite	6.3	0.3	0.2
Zone B	136	6.1	3.9
Mudstone	26.2	0	0
Sandstone	12.7	0.9	0.7
Limestone	71.9	3	1.7
Dolomite	25.1	2	1.4
Zone C	94.7	5.5	3.6
Mudstone	21.4	0	0
Sandstone	7.6	0.6	0.4
Limestone	28.8	1.6	0.9
Dolomite	36.7	3.2	2.2
Zone D	92.8	3	2.4
Mudstone	68.5	0	0
Sandstone	1.7	0.2	0.2
Limestone	5	0.5	0.4
Dolomite	17.4	2.1	1.8
Total	439.7	19.3	12.4
Mudstone	126.2	0	0
Sandstone	107.6	5.5	3
Limestone	120	5.8	3.5
Dolomite	85.7	7.9	5.8

Table 1: Summarizes the pore volume and hydrocarbon pore volume (HCPV) of the Wolfcamp by stratigraphic Zone and rock type. HCPV stratigraphically increases moving up through the section in Zone B-D. The rock type with the highest pore volume and HCPV is dolomite, even though it is least represented within the Wolfcamp interval in terms of bulk volume.

quality is associated with limestones given their low values for ϕ_t, ϕ_e, and BI and relatively high S_w (with p-impedance range of 48,000-68,000 (ft*s)(g/cc)).

DISCUSSION

Rock Types and Petrophysical and Geomechanical Properties related to Reservoir Quality

Within the study area, the Wolfcamp Formation exhibits stratigraphic variability and spatial distribution of mineralogy, rock types, and petrophysical and geomechanical properties. As a result, preferential intervals of ideal reservoir quality are identified (for this discussion, mudstone is considered non-reservoir). Stratigraphically, carbonate-rich minerals (calcite and dolomite) and rock types (limestone and dolomite, respectively) increase upward through the section in Zone B-D then transition to clastic-rich (quartz; sandstone) composition in Zone A. The stratigraphic variability in mineral composition and rock types is reflected in the distribution of BI. Generally higher BI correspond to high distribution of quartz and dolomite mineral-derived rock types (sandstone and dolomite). ϕ_e is variable throughout the stratigraphic section but show preferential distribution in rock types that contain high or low values; higher values of ϕ_e correspond to dolomite while lower ϕ_e values correspond to limestone. Stratigraphically, S_w increases moving up the section in Zone A-D (mean= 48%, 36%, 32%, to 16%). The stratigraphic variability among rock types and petrophysical and geomechanical properties associate dolomite with high ϕ_e, high BI and low S_w, limestone with low ϕ_e, low BI and high S_w, and sandstone with low ϕ_e, high BI and high S_w. Additionally, hydrocarbon pore volume was highest for dolomite, irrespective of bulk volume. In terms of rock type, dolomite illustrates a balance of ideal reservoir quality while limestone and sandstone illustrate poor reservoir quality. The spatial distribution and percent of rock types and their associated petrophysical and

geomechanical properties identify an ideal interval to land horizontal wells. Zone A and D are primarily composed of sandstone and mudstone (respectively) which do not exhibit ideal reservoir quality. Zones B and C are more complex as they are primarily composed of limestone (poor reservoir quality) and dolomite (ideal reservoir quality). In Zones B-C limestones increase in proportion and migrate to the north-northwest while dolomites do not show a distinct migration trend (Figure 17). Given the stratigraphic and spatial distribution of significant petrophysical and geomechanical properties the ideal rock type and interval to land horizontal wells would be dolomite in Zone C. Zone C is primarily composed of high ϕ_e, pore volume, HCPV, BI, and low S_w associated with dolomite (Appendix F).

Utilizing ρ_{maa}-U_{maa} Interpretation of Mineral Composition

Determining mineral composition is essential for the Wolfcamp Formation due to their variability in associated reservoir qualities. Broad classification of rock types such as carbonate and clastic are too general, as reservoir quality within the carbonates vary significantly. ρ_{maa}-U_{maa} analysis provide a solution by distinguishing the calcite and dolomite compositions within the total carbonate percentage. The variability of both reservoir quality and mineral composition is illustrated moving up the stratigraphic section. The base of the Wolfcamp is primarily composed of clay-rich composition associated with low ϕ_e, BI and S_w resulting in non-reservoir rock. Moving up the section the clay content decreases as carbonate-rich minerals (calcite and dolomite) compose nearly the entire section. In terms of calcite, the spatial distribution of petrophysical and geomechanical properties illustrate low ϕ_e, low BI and high S_w, while dolomite is associated with high ϕ_e, high BI, and low S_w. Toward the top of the section, carbonate-rich minerals decrease and quartz dominates the section with associated low ϕ_e, high BI and high S_w (Figure 3). Given the spatial distribution of significant petrophysical and geomechanical

properties, the distinction between dolomite and calcite mineral composition is essential for determining the interval with ideal reservoir quality. Zone B has the highest carbonate percentage within the Wolfcamp however it is primarily composed of calcite-derived rock type (limestone) which is associated with poor reservoir quality while Zone C contains a lower percentage of carbonate-rich composition but has the highest dolomite-derived rock type (dolomite) and associated high reservoir quality (Figure 3). Targeting the interval with the highest carbonate percentage would not result in drilling ideal reservoir quality as determined by utilizing ρ_{maa}-U_{maa} analysis.

Limitations

The limitations of this study include the lack of core to provide lithologies and lithofacies. Using ρ_{maa}-U_{maa} analysis and V_{sh} cut offs provide general rock types that could be better defined with core examination. Core data provides a means to calibrate the well logs and provide data such as TOC and XRD measurements to reduce uncertainty associated with rock-type interpretation. Core description provides sedimentary structures, biological features, and aide an interpretation for the environment of deposition and depositional cycles. In terms of thin sections, alizarian red-S and potassium ferricyanide stained thin sections could validate the mineral distinction between the calcite and dolomite minerals. Additionally, thin section analysis provides essential information such as grain size, framework grains and matrix components. In terms of the reservoir models, there is a limitation in vertical resolution because the Wolfcamp stratigraphic zones were not mapped in the seismic data due to a lack of continuous reflectors.

CONCLUSIONS

The Wolfcamp Formation on the Northwest Shelf, Delaware Basin is comprised of carbonate and clastic debris flows that form a low angle slope-to-basin depositional environment

and illustrates a variation of stratigraphic thickness, mineralogies, rock types, and petrophysical and geomechanical properties. The Wolfcamp in the study area dips to the east-southeast and varies in thickness from 200-1000 ft (60-304 m). It is informally divided into 4 operational units, zones A-D, that proportionally thicken to the east-southeast. ρ_{maa}-U_{maa} multi-mineral analysis and a V_{sh} cut off were used to derive rock types (1) mudstone (2) sandstone (3) limestone, and (4) dolomite. Each zone contains a dominant rock type composition; Zone A (sandstone), Zone B (limestone), Zone C (dolomite), and Zone D (mudstone). A relationship between rock types and well-log p-impedance suggest that ranges in p-impedance values approximately correlate to rock types.

A post-stack inversion yielded an impedance volume and was used to spatially distribute rock types based on ranges in p-impedance associated with each rock type. Limestone and mudstone show distinct distribution trends while sandstone and dolomite do not. The spatial distribution of reservoir quality was analyzed using seismically constrained rock-type, petrophysical, and geomechanical properties models. The Wolfcamp Formation in this study area displays both stratigraphic and lateral variability of reservoir quality.

The stratigraphic variability and spatial distribution of significant petrophysical and geomechanical properties illustrate a relationship among ideal reservoir quality and corresponding rock types. Pore volume and hydrocarbon pore volume (HCPV) are highest within dolomite. Dolomite contains an ideal balance of reservoir quality in terms of ϕ_e, pore volume and HCPV. Zone C contains low S_w, high BI and the highest proportion of dolomite with associated ideal reservoir quality.

Based on the results of this study, Zone C contains petrophysical and geomechanical characteristics associated with higher reservoir quality within the Wolfcamp Formation. This

study is important for research done on the Wolfcamp Formation because it provides assessment of the stratigraphic and lateral distribution of significant mineralogies, rock types, and petrophysical and geomechanical properties in this area of the Northwest Shelf, Delaware Basin.

REFERENCES

Adams, J. E., 1965, Stratigraphy-Tectonic Development of Delaware Basin: AAPG Bulletin v. 48, no. 11, p. 2140-2148.

Archie, G. E., 1947, Electrical Resistivity an Aid in Core-Analysis Interpretation, AAPG Bulletin, v. 31, no. 2 p. 350-366.

Asquith, G. B., 2016, Permian Wolfcamp Interesting Log Interpretation Problem: Search and Discovery Article #41896, Website accessed March 2020.

Asquith, G. B. and C. R. Gibson, 1982, Basic Relationship of Well Log Interpretation: Chapter 1 in Basic Well Log Analysis for Geologist, Methods in Exploration.

Barnes, A. E., 2007, A tutorial on complex seismic trace analysis: Geophysics, 72, W33–W43.

Bassiouni, Z., 1994, Gamma Ray Absorption Logs: Litho-density in (eds.) P. A. Schenewerk, D. A. Pert, Theory, Measurement and Interpretation of well logs: SPE, v. 4, p.159-167.

Bickley, T., 2019, High Resolution Sequence Stratigraphy and Seismic Stratigraphy if the Leonardian Bone Spring Formation Delaware Basin, Southeast New Mexico, University of Oklahoma Master's Thesis.

Cook, H. E., 1983, Sedimentology of some allochthonous deep-water carbonate reservoirs, Lower Permian, west Texas: Carbonate debris sheets, aprons, or submarine fans? (abs.): AAPG Bulletin, v. 67, p. 442.

Dommisse, R., L. Sivila, F. Male, H. S. Hamlin, 2018, The Value of Building a Multiscale, Regional Geomodel for Reserves Assessment of the Midland Basin: Economic Geology, Jackson School of Geosciences, The University of Texas at Austin, URTeC.

Dommisse, R., X. Janson, F. Male, B. Price, S. Payne, A. Lewis, 2018, An Integrated, Multiscale Geomodel of the Northern Delaware Basin in URTeC: SEG, AAPG, SPE.

Doveton, J. H., 1999, Basics of oil and gas log analysis: Kansas Geological Survey, Retrieved from http://www.kgs.ku.edu/PRS/pdf/oilgas_log.html, Accessed May 15, 2020.

Ewing, T. E., R. T. Budnik, J. T. Ames, D. M. Rider, 1990, Tectonic map of Texas: Bureau of Economic Geology, University of Texas at Austin.

Farfour, M., Yoon, W. and Kim, J. (2015). Seismic attributes and acoustic impedance inversion in interpretation of complex hydrocarbon reservoirs. Journal of Applied Geophysics, 114, p.68-80.

Frenzel, H. N., R. R. Bloomer, R. B. Cline, J. M. Cys, J. E. Galley, W. R. Gibson, S. Thompson III, 1988, The Permian Basin region. Sedimentary cover- North American craton: U.S.: Geological Society of America, the Geology of North America, v. 2 p. 261-306.

Galley, J. E., 1958, Oil and Geology in the Permian Basin of Texas and New Mexico: North America: Habitat of Oil, AAPG special volume, p. 395-446.

Gaswirth, S. B., 2017, Assessment of continuous oil resources in the Wolfcamp shale of the Midland Basin, Permian Bain Province, Texas, 2016: U.S. Geological Survey Open File-Report 2017–1013, p. 14.

Handford, C. R., 1981, Sedimentology and genetic stratigraphy of Dean and Spraberry Formations (Permian), Midland Basin, Texas: AAPG Bulletin, v. 65, no. 9, p. 1602-1616.

Handford, C. R. and R. G. Loucks, 1993, Carbonate depositional sequences and systems tracts-Response of carbonate platform to relative sea-level changes in R. G. Loucks and J. F. Sarg, eds., Carbonate sequence stratigraphy: Recent development and applications: AAPG Memoir 57, p.3-41.

Hayes, P. T., 1964, Geology of the Guadalupe Mountains New Mexico: United States Geological Survey, Professional Paper v. 446.

Hills, J. M., 1984, Sedimentation, tectonism, and hydrocarbon generation in Delaware Basin, west Texas and southeastern New Mexico: AAPG Bulletin, v. 68, no. 3, p. 250-267.

Hobson, J. P., C. D. Cadwell, D. F. Toomey, 1985, Sedimentary Facies and Biota of Early Permian Deep-Water Allochthonous Limestone, Southwest Regan County, Texas: SEPM, Deepwater Carbonates.

Hurst, J. M., and F. Surlyk, 1984, Tectonic control of Silurian carbonate-shelf margin, morphology and facies, North Greenland: AAPG Bulletin, V. 68, p. 1-17.

Jafari, M., Nikrouz, R., A. Kadkhodaie, 2017, Estimation of acoustic-impedance model by using model-based seismic inversion on the Ghar Member of Asmari Formation in an oil field in southwestern Iran: SEG, The Leading Edge.

Janson, X., B. Price, C. Zahm, J. Covault, R. Dommisse, D. Dunlap, 2019, Seismic Geomorphology of the Permian Shelf Margin Slope and Basin in the Northern Delaware Basin: AAPG, Search and Discovery Article #90350.

Kerans, C., and W. M. Fitchen, 1995, Sequence hierarchy and facies architecture of a carbonate-ramp system: San-Andreas Formation of Algerita Escarpment and western Guadalupe Mountains, West Texas and New Mexico: Bureau of Economic geology, University of Texas at Austin, v. 235.

Kosters, E. C., D. G. Bedout, S. J. Seni, C. M. Garret, L. F. Brown, H. S. Hamlin, N. Tyler, 1989, Atlas of major Texas gas reservoirs.

Kvale, E. P., C. M. Bowie, C. Flenthrope, C. Mace, J. M. Parrish, B. Price, S. Anderson, W. A. DiMichele, 2020, Facies variability within a mixed carbonate-siliciclastic sea-floor fan (upper Wolfcamp Formation, Permian, Delaware Basin, New Mexico): AAPG Bulletin, v. 10, no. 3, p. 525-563.

Lindseth, R. O., 1979, Synthetic sonic logs — A process for stratigraphic interpretation: Geophysics, 44, no. 1, 3–26.

Loucks, R. G., A. A. Brown, C. W. Achauer, D. A. Budd, 1985, Carbonate gravity flow sedimentation on low-angle slopes off the Wolfcampian Northwest Shelf of the Delaware Basin in (eds.) P. D. Crevello, P. M. Harris, Deep-water carbonates; build ups turbidities, debris flows and chalks, a core workshop: SEPM Core Workshop, v. 6, p. 56-92.

Market, J., and T. J. Parker, 2011, Reliable LWD Calliper Measurements: SPE, SPE Offshore Europe Oil and Gas Conference and Exhibition.

Mazzulo, S. J., 1984, Foreshelf carbonate facies mosaic, Permian Midland Basin, Texas (abs): SEPM 1st Annual Midyear Mtg., San Jose, California.

Moede, I., 2018, Lithofacies and Chemostratigraphy of the Upper Wolfcampian in the southeastern Delaware Basin, Pecos County, Texas, University of Texas Master's Thesis.

Oriel, S. S., D. A. Meyers, E. J. Crosby, 1967, West Texas Permian Basin Region in E. D. McKee, S. S. Oriel, Paleotectonic Investigation of the Permian System in the United States, United States Geological Survey: Professional Paper, v. 515, p. 21- 60.

Playton, T. E., and C. Kerans, 2002, Slope and toe-of-slope deposits shed from a late Wolfcampian tectonically active carbonate ramp margin: Gulf Coast Association of Geological Societies, v. 52, p. 811–820.

Pranter, M. J., N. F. Hurley, T. L. Davis, 2004, Anhydrite distribution within a shelf-margin carbonate reservoir, San Andres Formation, Vacuum Field, New Mexico, USA: Petroleum Geoscience, v. 10, p. 43-52.

Scotese, C. R., 2014, Atlas of Permo-Carboniferous Paleogeographic Maps (Mollweide Projection), Maps 53-64, V. 4, The Late Paleozoic, PALEOMAP Atlas for ArcGIS, PALEOMAP Project, Evanston, IL.

Shumaker, R. C., 1992, Paleozoic Structure of the Central Basin Uplift and Adjacent Delaware Basin, West Texas: AAPG Bulletin, v. 76, no. 11, p. 1804-1824.

Silver, B. A., and R. G. Todd, 1969, Permian cyclic strata, northern Midland and Delaware Basins, west Texas and southeastern New Mexico: AAPG Bulletin, v. 53, no. 11, p. 2223-2251.

Theologou, P. N., D. McCarty, T. Fisher, A. Derkowski, R. Stokes, A. Ollila, 2015, Mineral-Chemistry Quantification and Petrophysical Calibration for Multi-Mineral Evaluation, AAPG International Conference & Exhibition.

Thomas, E. C., and S. J. Stieber, 1975, The Distribution of Shale in Sandstone and its Effects Upon Porosity: SPWLA, SPWLA 16th Annual Logging Symposium.

UH Energy, 2019, Opportunities and Challenges in the Permian: University of Houston, UH Energy White Paper Series, Retrieved from https://www.uh.edu/uh-energy/research/white-papers/white-papers-files/permian-basin-02-2019.pdf.

U.S. Department of Energy, 2018, Independent Statistics and Analysis, Permian Basin, Wolfcamp Shale Play: Geology Review, Retrieved from https://www.eia.gov/maps/pdf/PermianBasin_Wolfcamp_EIAReport_Oct2018.pdf

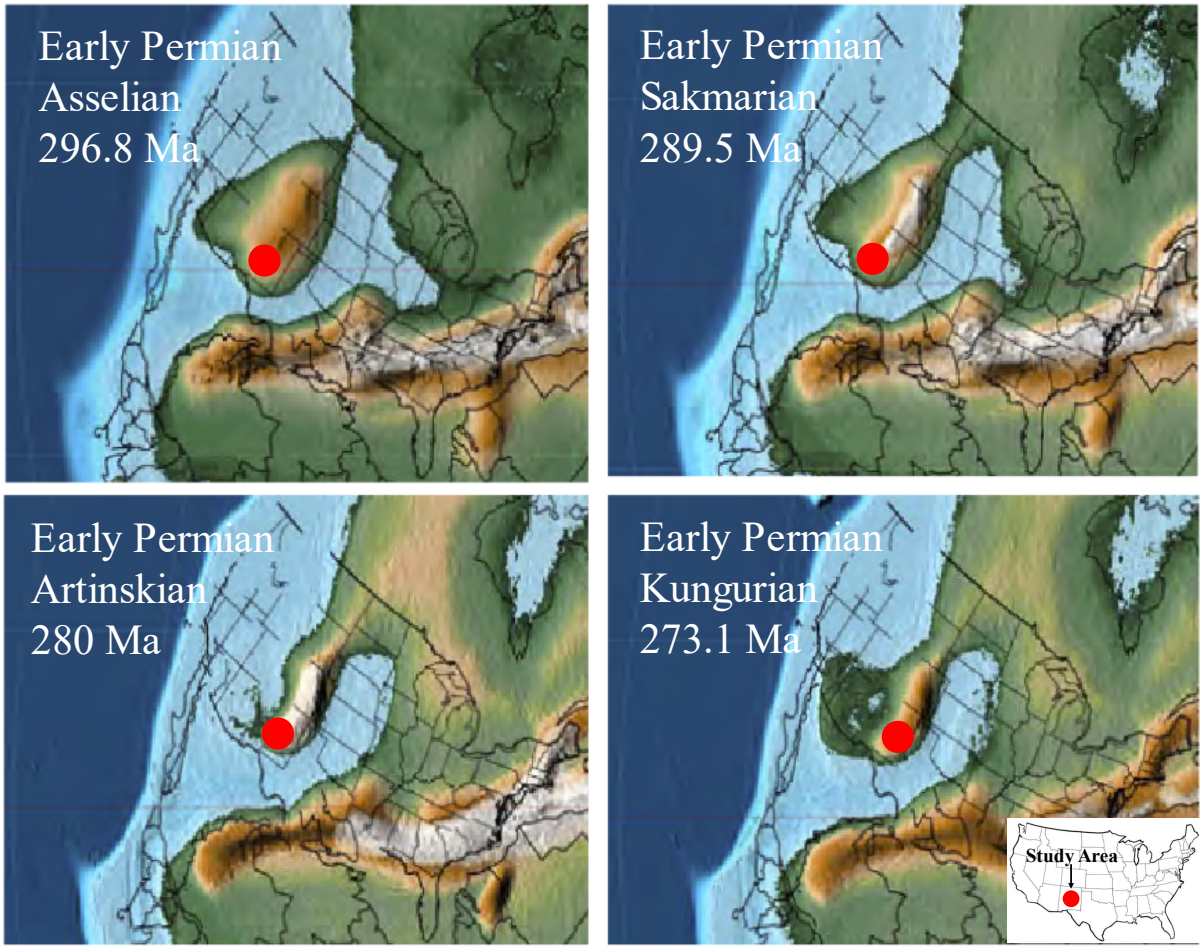
U.S. Department of the Interior, 2018, USGS Identifies Largest Continuous Oil and Gas Resource Potential Ever Assessed: U.S. Department of the Interior, Retrieved from https://www.doi.gov/pressreleases/usgs-identifies-largest-continuous-oil-and-gas-resource-potential-ever-assessed

Vertrees, C. D., 1953, Developments in West Texas and Southeast New Mexico in 1952: AAPG Bulletin, v. 37, no. 6, p. 1358-1375.

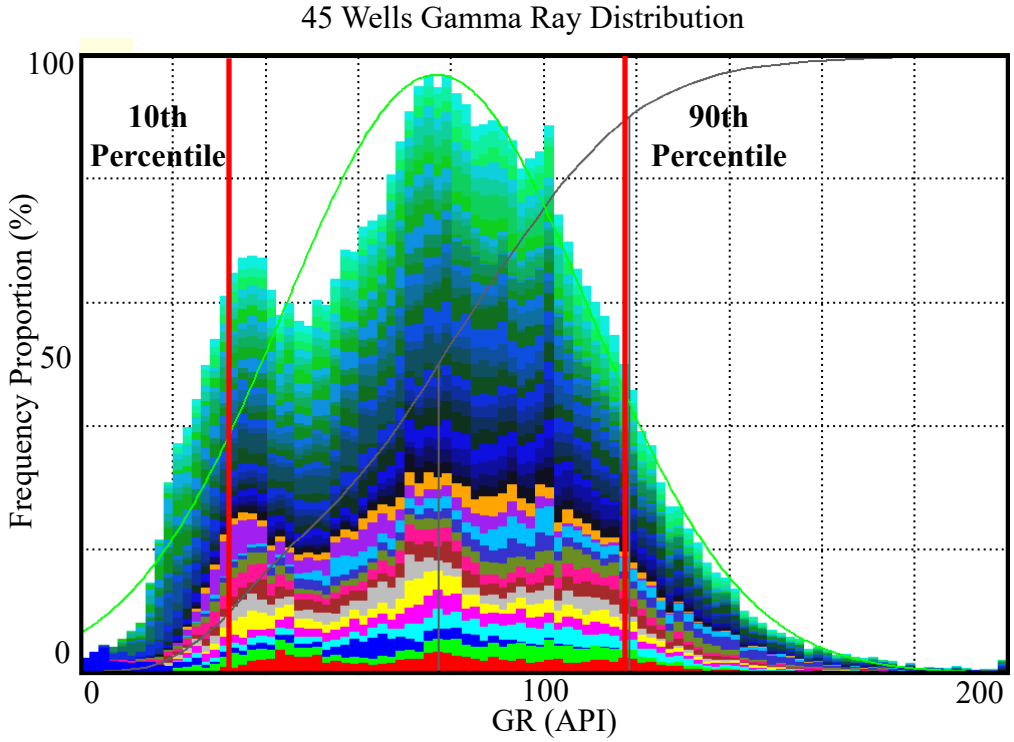
Wang, F. P., and J. F. Gale, 2009, Screening for Shale-Gas Systems: Gulf Coast Association of Geological Societies Transactions, v. 59, p. 779-793.

Yang, K.M., and S.L. Dorobek, 1995, The Permian Basin of West Texas and New Mexico: Flexural Modeling and Evidence for Lithospheric Heterogeneity Across the Marathon Foreland in S.L. Dorobek, G.M. Ross Stratigraphic Evolution of Foreland Basins: SEPM Special Publication no. 52.

APPENDIX



Appendix A: These map illustrate the paleogeography during the early Permian, the same time the Wolfcamp Formation was being deposited. During this time most of the Delaware Basin was underwater and the paleo-water depth was around 1000 ft (300 m). The Wolfcamp Formation on the Northwest Shelf of the Delaware Basin (Figure 1) formed in a low-angle (<1°) slope-to-basin depositional environment and is primarily composed of carbonate and clastic sediment gravity flows (Cook, 1983; Scotese, 2014; Kvale et. al., 2020).



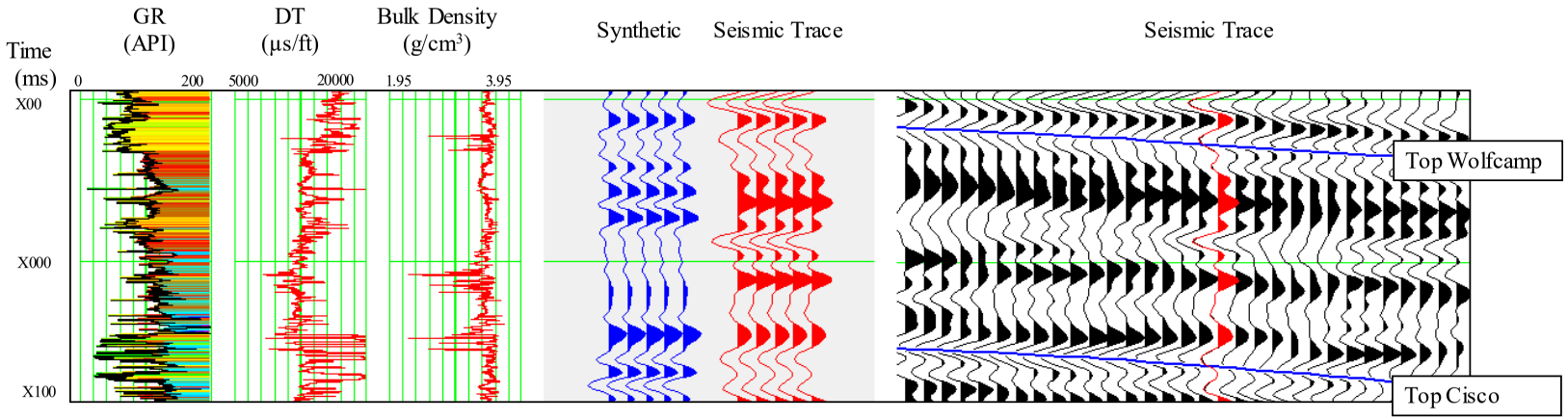
Appendix B: The gamma-ray distribution for all 45 well within the study area was used to identify the sandstone and shale GR API baselines to compute the Shale Index (I_{sh}). The sandstone baseline corressponds to the 10th percentile (38 API) while the shale baseline corresponds to the 90th percentile (118 API).

Appendix C: The hydrocarbon pore thickness (HCPT) was calculated by multiplying the effective hydrocarbon saturated pore space to the net rock thickness (Equation 1). The effective hydrocarbon pore space is defined by multiplying the ϕ_e and S_o (1-S_w). The net rock thickness is computed by multiplying the total thickness of the interval by the net-to-gross ratio of reservoir (net) rock thickness. In this case non-reservoir rock is determined by the amount of shale present indicated by the V_{sh} log. The net-to-gross ratio is represented by the percentage of V_{sh} beginning with 0% to 100%, increasing by 5% each time. For example, starting with 0% V_{sh} would indicate that the entire interval consists of reservoir rock and the HCPT would be high. As the amount of V_{sh} increases, the amount of reservoir rock decreases, as does the HCPT. Another example, if 85% V_{sh} was used as the net-to-gross ratio, the amount of reservoir rock would be 15% resulting in low HCPT. Once the HCPT was calculated for 0 to 100% V_{sh} (increasing by 5% each time), they were cumulatively added and normalized out of 100%

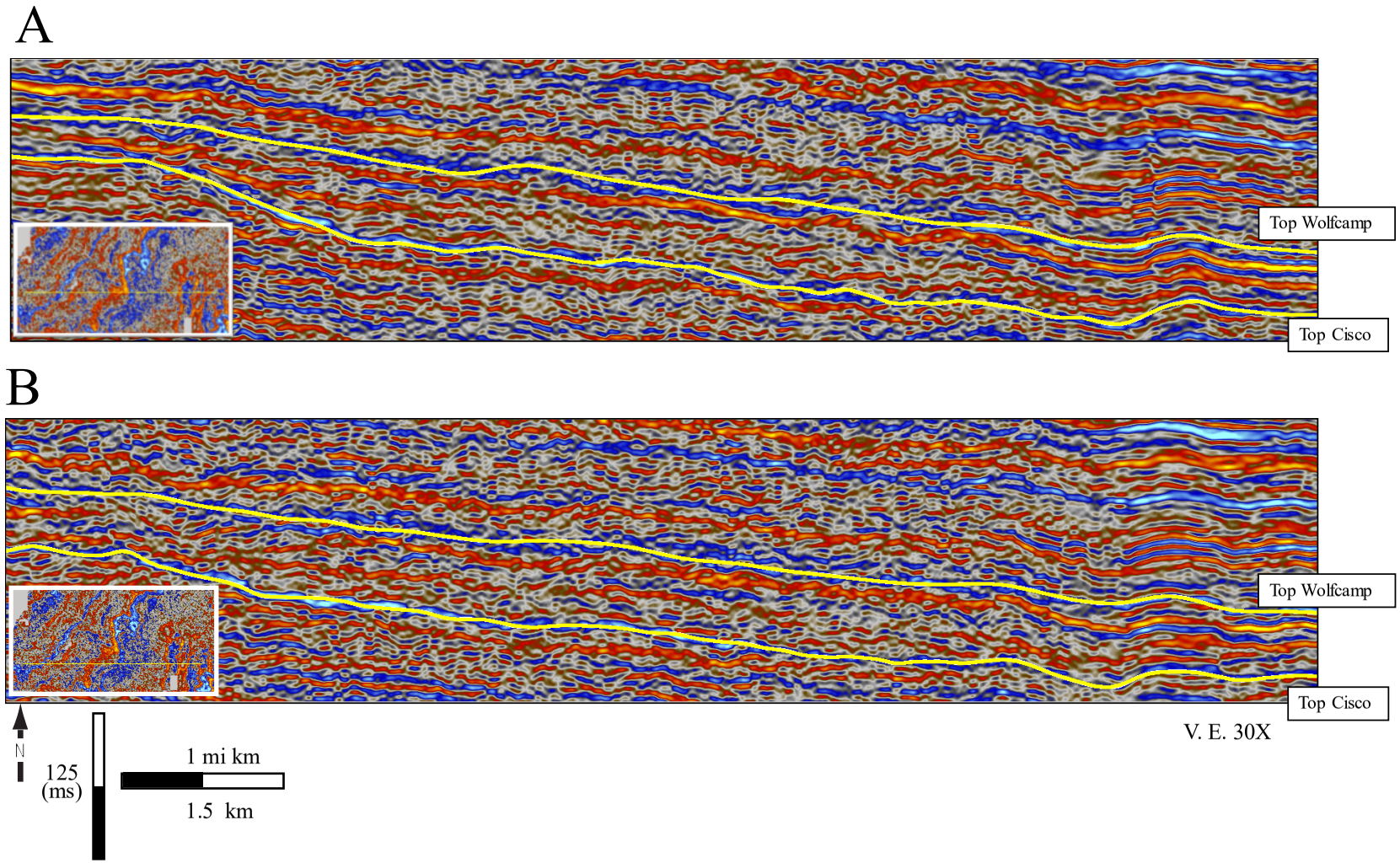
$$HCPT = \phi_e * S_o * GRT * N/G \quad (1)$$

where,

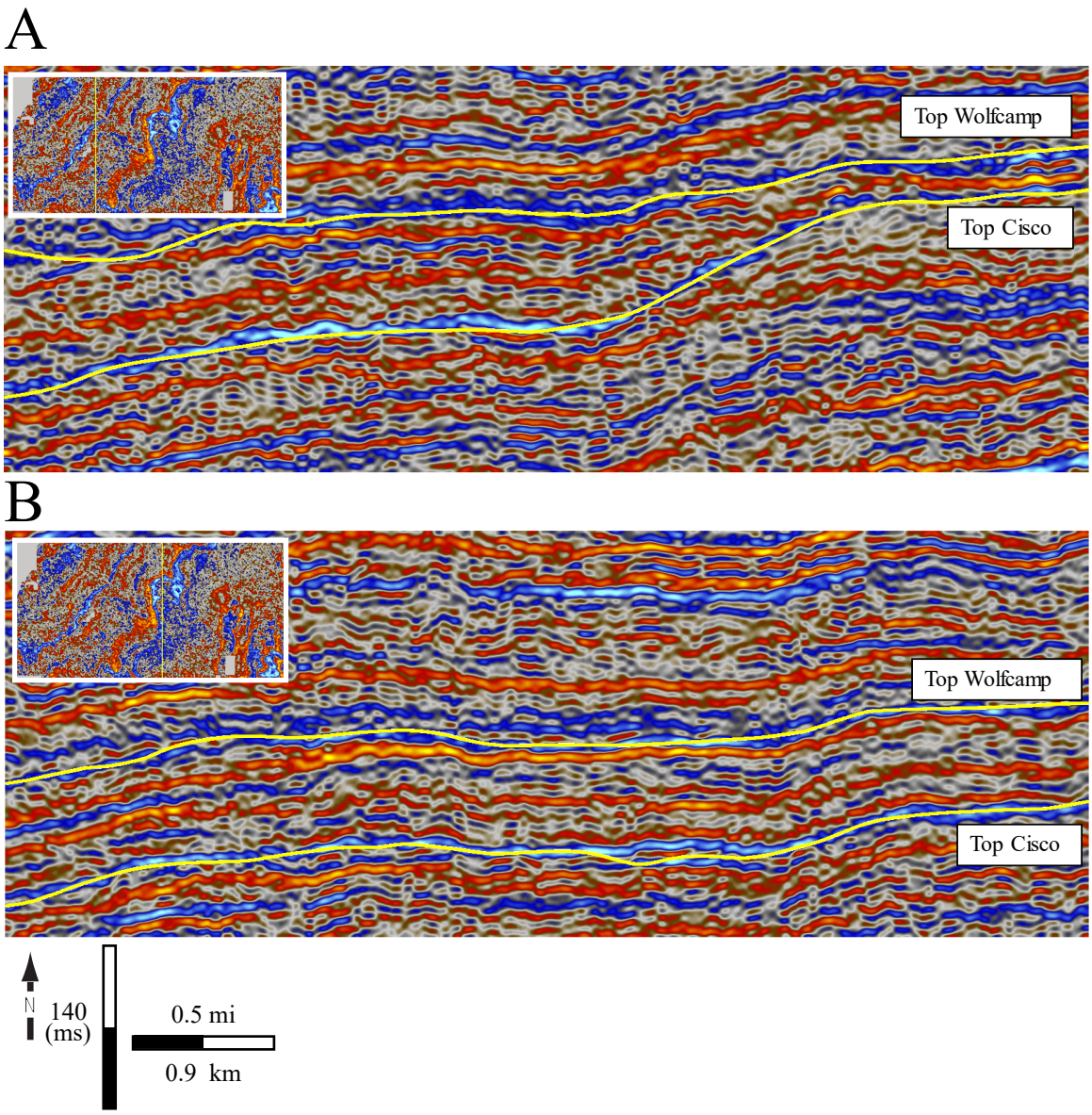
- ϕ_e, Effective porosity (v/v)
- S_o, Hydrocarbon saturation (v/v)
- GRT, Gross thickness of interval (ft)
- N/G, Net to gross ratio



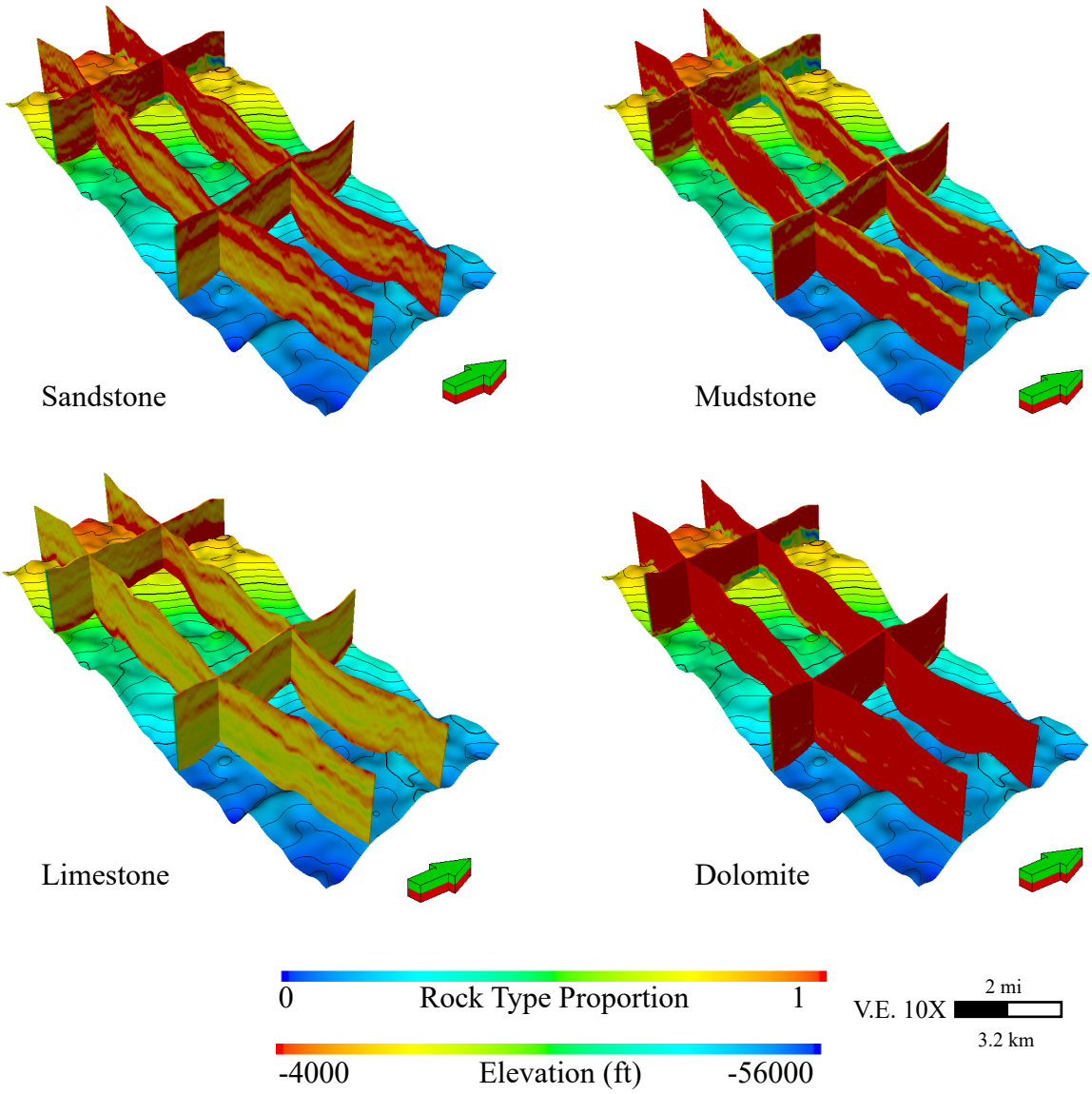
Appendix D1: Four seismic-to-well ties were done to relate the Zone tops (in depth; SSTVD) to seismic amplitude reflectors (in time; ms) using synthetic traces. The top of the Wolfcamp and Cisco (base Wolfcamp) formations were identified in the 3D seismic survey as distinct continuous low amplitude reflectors and their horizons were mapped across the study area.



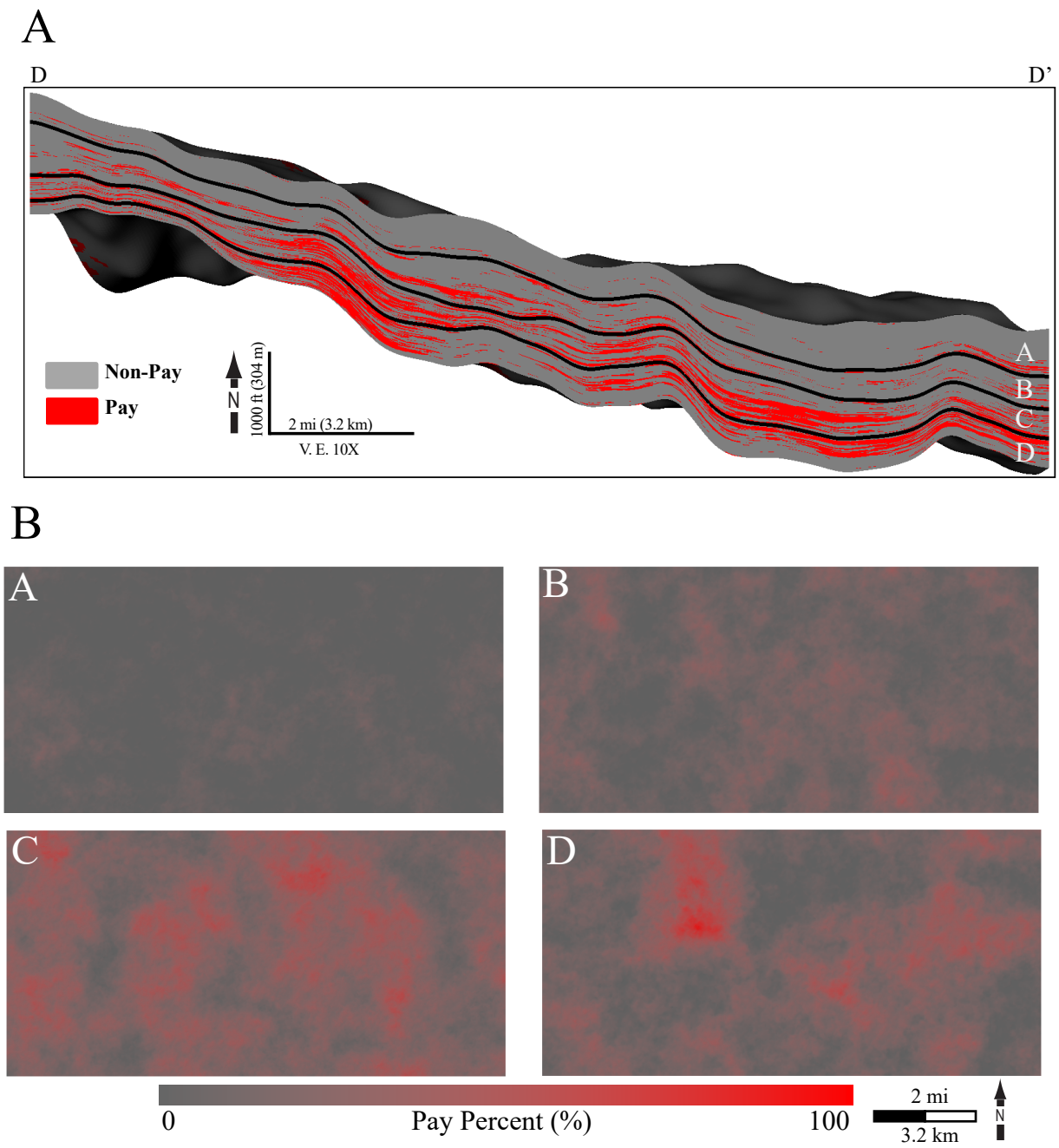
Apendix D2: A and B illlustrate the vertical resolution of the seismic data. The top of the Wolfcamp and Cisco Formations were identified by continuous relectors however the stratigraphic Wolfcamp zones could not be interpreted.



Apendix D3: A and B illlustrate the vertical resolution of the seismic data. The top of the Wolfcamp and Cisco Formations were identified by continuous relectors however the stratigraphic Wolfcamp zones could not be interpreted.



Appendix E: The trend volumes were derived using the depth converted p-impedance volume and the ranges in p-impedance that correspond to each rock type. The volumes are scaled in such a way that 1 (red) suggest high probability of specified rock type proportion and 0 (blue) suggest low probability of specified rock type proportion. Trends for limestone and dolomite are more distinct because their ranges in p-impedance have the greatest contrast between each other. The p-impedance ranges for sandstone and dolomite are similar to one another resulting in less distinct trend volumes.



Appendix F: A) Based on petrophysical and geomechanical analysis favorable reservoir quality is defined by the dolomite rock type, $\phi_e > 0.04$ v/v, $S_w < 0.4$ v/v, BI> 0.6 v/v. The stratigraphic variability and spatial distrubution these qualities is represent by the pay model. B) displays the average pay percentage per zone as the following A) Zone A contains ~3% (7 ft), B) Zone B contains ~12% (36 ft), C) Zone C contains ~26% (54 ft), D) Zone D contains ~19% (37 ft).